Straggling in thin silicon detectors

Hans Bichsel

1211 22nd Avenue East, Seattle, Washington 98112

Experimental and theoretical data for dielectric functions, x-ray absorption coefficients, and generalized oscillator strengths needed for a description of the energy-loss spectrum of fast charged particles in solid silicon are given. Theories used to calculate spectra of total energy loss ("straggling spectra") are described. The convolution method is used to calculate straggling functions for thin silicon absorbers. They are compared with those obtained from other theories (Landau). For relativistic particles ($\gamma > 100$), the Vavilov-Shulek theories give incorrect functions for absorbers of thicknesses $t < 1$ mm. The conversion of energy-loss spectra into ionization spectra is discussed, and the latter are compared with experimental functions. Good agreement is found between calculated and observed functions for electrons, mesons, protons, and their antiparticles and for α particles. From this agreement, the error (1σ) of the theoretical values of the most probable energy loss Δ_p and the full width at half maximum, w, is estimated to be less than $\pm 1\%$.

CONTENTS

LIST OF SYMBOLS AND CONSTANTS

Numerical values actually used are given for silicon. They are not necessarily the best reference values.

A	atomic mass of target atom, 28.086
$A(E)$	integral over generalized oscillator strength, Eq. (2.11)
a_0	Bohr radius, 0.052 917 7 nm
B	Bethe's stopping number (also see L)
$C(\beta)$	shell correction
c	speed of light
dT/dt	stopping power
d_1, d_2	coefficients used in the asymptotic cross section, Eq. (3.4)
E	energy loss of incident particle in a single collision
E_f	Fermi energy, 12.46 eV
E_M	maximum energy loss
E_a	plasmon energy for all electrons, 31.048 eV
E_p	plasmon energy for M-shell electrons, 16.7 eV
e	electron charge
$F(E,K)$	matrix element for longitudinal excitations
$f(E,0)$	dipole oscillator strength

$f(E,K)$	generalized oscillator strength
$f(\Delta)$	energy-loss straggling function
$f_L(\lambda)$	Landau straggling function
$G(E,K)$	matrix element for transverse excitations
I	logarithmic average excitation energy, 174 eV
I_1	logarithmic average excitation energy, weighted by E, 2480 eV
Im	imaginary part of a complex function
J	ionization = number of ion pairs produced
K	change in momentum of incident particle
K_M	maximum value of K
K_m	minimum value of K
k	coefficient of extinction, also constant of Rutherford cross section, $k=2.55\times10^{-19}z^2$ eV/atom
L	stopping number in Lindhard nomenclature (see B)
M	mass of incident particle, electron: 0.511 004 MeV; pion: 139.578 MeV; proton: 938.256 MeV; alpha: 3727.328 MeV
M_ν	moments of cross section $\sigma(E)$
M'_ν	moments of Rutherford cross section $\rho(E)$
M_ν	νth moment of collision spectrum
m	rest mass of electron, $mc^2=0.511\,004$ MeV, also average number of collisions $m=\langle n\rangle$
N	number of particles
N_A	Avogadro's number, 6.0222×10^{23}/mole
N_a	number of atoms per unit volume, 4.9938×10^{22} cm^{-3}
n	index of refraction, also number of collisions of a particle in passing absorber
$P(n)$	Poisson distribution function
Q	energy of an electron with momentum K
Ry	Rydberg, 13.6058 eV
r_0	classical electron radius, $2.817\,939\times10^{-13}$ cm
T	kinetic energy of incident particle
t	absorber thickness
v	speed of the incident particle
v_0	Bohr speed, $c/137$
W	energy per ion pair, 3.68 eV for electrons
w	full width at half maximum of a straggling function
w_i	full width at half maximum of an ionization function
w_L	full width at half maximum of a Landau function
w_S	full width at half maximum of a Shulek function
w_x	full width at half maximum of experimental straggling function
w_n	full width at half maximum of experimental noise function
Z	atomic number of target atom, 14
Z_{eff}	effective nuclear charge
z	charge number of incident particle
β	v/c
Γ	Euler constant, 0.577 215
γ	$(1-\beta^2)^{-1/2}$, also width of free-electron plasmon function, ≈3.5 eV
Δ	total energy loss (sum over all E)
Δ'	total energy deposition in absorber
$\langle\Delta\rangle$	mean total energy loss
Δ_p	most probable total energy loss
${}_x\Delta_p$	experimental value of most probable energy deposition
${}_i\Delta_p$	theoretical value of most probable energy deposition
Δ_M	largest total energy loss under consideration
$\delta(\beta)$	density effect function
δ	a small number
$\delta(E,K)$	Kronecker delta
δ_2	$M_2-M'_2$, "resonance" correction term for Shulek $f(\Delta)$
$\varepsilon(E,K)$	complex dielectric constant of material
Θ	binding energy of electrons in atom
κ	Vavilov parameter, ξ/E_M
λ	Landau energy-loss variable
$\mu(E)$	x-ray attenuation coefficient
$\phi(J)$	experimental ionization spectrum
ρ	density of absorber, 2.329 g/cm^3
$\rho(E)$	Rutherford collision cross section
$\rho_r(E)$	relativistic Rutherford collision cross section
σ	standard deviation of a Gaussian
σ_n	standard deviation of noise contribution
σ_T	total collision cross section
$\sigma(E)$	collision cross section as function of energy loss E
$\sigma_l(E)$	collision cross section for longitudinal excitations
$\sigma_t(E)$	collision cross section for transverse excitations
$\sigma_u(E)$	collision cross section for large K
ξ	Landau parameter
$\xi(E,K)$	longitudinal excitation cross section
$\tau(E,K)$	transverse excitation cross section
ω	frequency of optical radiation

I. INTRODUCTION

Thin silicon detectors are used in nuclear and particle physics for the observation of the transit of charged particles. The ionization J (i.e., the number of electron-hole pairs) produced in the detector is recorded for each particle passing through it. It is related to the total energy loss Δ of the particle. Both Δ and J are stochastic quantities. The probability density functions $f(\Delta)$ and $\phi(J)$ are usually called straggling functions. They may be characterized schematically by the value Δ_p of the most probable energy loss and the full width at half maximum w. Energy-loss straggling functions will be derived here, and their relation to the observed ionization straggling functions will be described. In particular, absolute values

of W, the energy needed to produce an electron-hole pair, will be determined. Frequently, it is desired to identify the passing charged particles from the observed functions (Bichsel, 1970b; Talman, 1979; Allison and Cobb, 1980). Therefore it is important to have a complete and accurate theory for them.

Functions for fast particles ($\beta=v/c>0.25$, i.e., 20-keV electrons, 5-MeV pions, and 30-MeV protons) and detectors with thicknesses less than 3 mm will be obtained, with the further restriction that the thickness t of the detector be small compared to the range of the incident particles ($\kappa<0.6$). For electrons, t must be so small that multiple-scattering corrections are unimportant (Berger *et al.*, 1969).[1] It is assumed that the silicon crystal is oriented such that channeling of the particles will not occur (Eisen *et al.*, 1972; Esbensen *et al.*, 1978). The only interactions considered are Coulomb interactions with electrons and collective modes of excitation in the material. The influence of bremsstrahlung will be discussed in Appendix I, though. Nuclear interactions are disregarded; they will be infrequent and will change the ionization spectrum very little. Angular deflections of the particles will also change $\phi(J)$ very little and therefore will not be considered (Scott, 1963; Bichsel, 1972; Bichsel *et al.*, 1982). Related problems were discussed by Ahlen (1980), who dealt with background material in more detail than is given here.

A fast charged particle in traversing matter loses energy in discrete amounts E in independent, stochastic single collisions. For very thin absorbers, these energy losses have been observed in electron-energy-loss spectroscopy (e.g., Perez *et al.*, 1977, Hinz and Raether, 1979; Chen *et al.*, 1980). In these experiments, the angular deflection, related to the change in momentum K of the incident particle, is also observed. The probability for the occurrence of these collisions is described by the doubly differential cross section $\sigma(E,K)$.[2] In thicker absorbers, a particle will experience i ($i=0,1,2,3,\ldots$) collisions, and it suffers a total energy loss

$$\Delta=\sum_i E_i \ . \tag{1.1}$$

For a theory of the straggling functions, it is necessary to consider the probability for the occurrence of collisions and the probability for a particular energy loss E. The latter is described by the singly differential cross section $\sigma(E)$, Eqs. (2.6) and (3.8); the former is related by the Poisson distribution, Eq. (6.1), to the total collision cross section M_0, Eq. (4.1).

In order to get correct straggling functions, it is thus necessary to determine $\sigma(E)$ accurately. The information needed for this is discussed in Secs. II–IV. Theories of energy-loss straggling functions are discussed in Secs. VI and VII, results are given in Sec. VIII, the relation of energy loss and ionization is discussed in Sec. IX, and comparisons of theory and experiments are made in Sec. X.

[1]The differences between measured and calculated spectra are at least partly explained by the ratio $r_p(e)$ of Table V.

[2]In some papers (Ferrell, 1956; Ashley, 1982) the expression "inverse mean free path" is used to designate the collision cross section.

II. INTERACTIONS OF CHARGED PARTICLES WITH MATTER

In solid silicon, energy losses to individual electrons (producing delta rays) and to collective excitations ("plasmons") are the major interactions to be considered for present purposes. The basic information about the interactions is usually given by the cross-section $\sigma(E,K)$ differential in energy loss E and momentum transfer K. The integral of $\sigma(E,K)$ over K is then used to obtain the cross-section differential in energy loss, $\sigma(E)$. It is convenient to discuss the cross sections separately for different atomic shells, for longitudinal and transverse excitations, and for small and large momentum transfers and energy losses. Their basic properties and the data needed to calculate them are discussed in this section. The theory used to calculate them in the Born approximation goes back to Bethe (1930). Fano (1963) reviewed it in detail, and his formulation is adopted here.

The Rutherford cross section was used in several derivations of straggling functions and is therefore given first. It represents a good approximation for large energy losses (Fig. 8, below).

A. Rutherford cross section

The nonrelativistic Rutherford cross section $\rho(E)$ for an energy loss E in the collision of a charged particle having charge ze, rest mass M, and speed v, with a free electron having charge $-e$ and rest mass m, in the laboratory system is given by (Evans, 1967; Bichsel, 1968; Inokuti, 1971; Inokuti *et al.*, 1978)

$$\rho(E)=\frac{2\pi z^2e^4}{mv^2E^2}=\frac{k}{\beta^2E^2} \tag{2.1}$$

with

$$k=\frac{2\pi z^2e^4}{mc^2}=2\pi r_0^2mc^2z^2$$
$$=2.5496\times10^{-19}z^2\ \text{eV cm}^2\ , \tag{2.2}$$

where $r_0=e^2/mc^2$ is the classical electron radius, mc^2 the electron rest mass, $\beta=v/c$, and c the speed of light (values for the constants are given in the List of Symbols). Since the electron receives all the energy E lost by the particle, the momentum transfer K is determined by E: $E=K^2/2m$. $\rho(E)$ does not depend on M. The relativistic equation is given in Eq. (3.5).

B. Atomic collision cross sections

For single atoms, Fano (1963) derived the following relativistic equation for $\sigma(E,\mathbf{K})$:

$$\sigma(E,\mathbf{K})=\rho(Q)Z[\xi(E,\mathbf{K})+\tau(E,\mathbf{K})](1+Q/mc^2)\ , \quad (2.3)$$

where $\mathbf{K}$ is the momentum transfer, $\rho(Q)$ is given by Eq. (2.1) with $Q=[(mc^2)^2+(cK)^2]^{1/2}-mc^2$, and Z is the number of electrons per atom. If the atom is ionized in the process, E and $\mathbf{K}$ are both shared by the electron and the recoil ion, and there is no simple relation between E and Q (see Figs. 3–7, below). The functions $\xi(E,\mathbf{K})$ and $\tau(E,\mathbf{K})$ are the longitudinal and the transverse excitation functions, defined by

$$\xi(E,\mathbf{K})=\frac{|F(E,\mathbf{K})|^2}{(1+Q/2mc^2)^2} \quad (2.4)$$

and

$$\tau(E,\mathbf{K})=\frac{|\boldsymbol{\beta}_t\cdot\mathbf{G}(E,\mathbf{K})|^2}{[1+Q/2mc^2-E^2/(2mc^2Q)]^2}\ , \quad (2.5)$$

with $F(E,\mathbf{K})$ and $G(E,\mathbf{K})$ the matrix elements for longitudinal and transverse excitations, and $\boldsymbol{\beta}_t$ the component of $\boldsymbol{\beta}=\mathbf{v}/c$ perpendicular to $\mathbf{K}$. The essential dependence on the speed and the charge of the incident particle thus appears only in $\rho(Q)$, while the properties of the material appear in $\xi(E,\mathbf{K})$ and $\tau(E,\mathbf{K})$. The sum of the two is called the "inelastic form factor." See Fano (1963) for further details. The dependence on v is not indicated explicitly in the symbol $\sigma(E,\mathbf{K})$. For collisions with small momentum transfer in the solid, the complex dielectric function $\varepsilon(\omega,K)$ will be used in the calculations of the collision cross section (see Sec. III.A).

The collision cross-section differential in energy loss E, $\sigma(E)$, is needed. It is calculated from $\sigma(E,K)$ with the following integral [an average over $\mathbf{K}$ is now assumed in $\xi(E,\mathbf{K})$ and $\tau(E,\mathbf{K})$]:

$$\sigma(E)=\int_{Q_m}^{Q_M}\sigma(E,K)dQ$$
$$=\frac{kZ}{\beta^2}\int_{Q_m}^{Q_M}\frac{[\xi(E,K)+\tau(E,K)]}{Q}\left[1+\frac{Q}{mc^2}\right]d\ln Q\ , \quad (2.6)$$

where $Q_M\approx 2mv^2$ [the exact equation is given in Eq. (3.6)] and $Q_m\approx E^2/Q_M$. The relation between K and Q is given below Eq. (2.3). The cross section $\sigma(E)$ depends on the speed v of the incident particle through the factor $1/\beta^2$ as well as through Q_m and Q_M. This dependence is not shown in the symbol $\sigma(E)$, but values of $\sigma(E)$ must be calculated for each speed.

For the present application, it is not practical to evaluate Eq. (2.6) for each energy loss and speed. Therefore the integral is evaluated separately for transverse and longitudinal excitations, and the following approximations are used.

For the transverse excitations, the matrix elements are large only near $K=0$ and, for large energy losses, near $K^2=E$. Thus, for small momentum transfers, Fano gave the approximation [Fano's Eq. (23)]

$$|\boldsymbol{\beta}_t\cdot\mathbf{G}(E,\mathbf{K})|^2\approx\beta_t^2 f(E,0)E/2mc^2\ . \quad (2.6a)$$

We note that β_t is equal to zero at $K=K_m$. For excitations in the solid, the corresponding equation will be given in Eq. (3.2). For intermediate values of Q, the contribution from transverse excitations is negligible,[3] because it is proportional to $Q/2mc^2$, Eq. (2.23). For large K and E, the approximation of Eq. (2.23) is used. Problems are encountered for the integral over longitudinal excitations, which are discussed next.

C. Bethe approach for longitudinal excitations

In order to conform to customary use (Manson, 1972; Miller *et al.*, 1983), atomic units will now be used. They are defined by $e=\hbar=m=1$, E in Ry=13.6 eV, K in units of $1/a_0$, where a_0 is the Bohr radius, v in units of $v_0=c/137$, and $Q=K^2$. The values of K_m and K_M are approximately $K_m=E/v$, $K_M=2v$ (Lindhard and Winther, 1964). Exact values were given by Inokuti (1971, 1978). Customarily, the oscillator strengths rather than the excitation functions have been used in the description of the cross sections. For the longitudinal excitations, for $Q\ll mc^2$, they are defined by

$$f(E,K)=E\xi(E,K)/K^2\ ; \quad (2.7)$$

$f(E,0)$ is called the dipole oscillator strength (DOS), and $f(E,K)$ the generalized oscillator strength (GOS). The longitudinal GOS $f(E,K)$ for $2p$ electrons of silicon as a function of K is shown below in Figs. 3 and 4 for two values of E. It is seen that $f(E,K)$ is practically constant for $Ka_0<1$. Thus the integral of Eq. (2.6) diverges for $Q_m\to 0$. The nature of the longitudinal excitations for small and intermediate energy losses (i.e., $E\ll mc^2$) can be understood easily if the integral over $\xi(E,K)$ of Eq. (2.6) is divided into two parts (Bethe *et al.*, 1950), corresponding to the definition of "distant" (or "resonance") and "close" collisions (Bohr, 1948; Lindhard and Winther, 1964; Bak *et al.*, 1987). This division shall be defined by a value K_1, chosen such that the difference $f(E,K)-f(E,0)$ is small for $K<K_1$. The integral can then be written as [we neglect $Q/mc^2\ll 1$ in Eq. (2.6)]

$$\sigma_l(E)[E\beta^2/(2kZ)]=\int_{K_m}^{K_1}f(E,0)d\ln K$$
$$+\int_{K_1}^{K_M}f(E,K)d\ln K$$
$$+\int_{K_m}^{K_1}[f(E,K)-f(E,0)]d\ln K\ , \quad (2.8)$$

where Q_M was replaced by K_M, Q_m by K_m, and $d\ln Q$ by $2\,d\ln K$.

The first integral can be evaluated as

$$f(E,0)\ln\frac{K_1}{K_m}\approx f(E,0)\ln\frac{vK_1}{E}\ . \quad (2.9)$$

[3] Additional remarks about transverse excitations can be found on p. 11 of Fano (1963).

The corresponding formulation for solid-state excitations will be given in Sec. III.A. For the second and third integrals, the abbreviation

$$A_1(E)\equiv\int_{K_1}^{K_M} f(E,K)d\ \ln K + \int_{K_m}^{K_1}[f(E,K)-f(E,0)]d\ \ln K \qquad (2.10)$$

is defined. A function $A(E)$ independent of particle speed can be defined by changing K_m to 0 and K_M to ∞:

$$A(E)=\int_{K_1}^{\infty} f(E,K)d\ \ln K + \int_{0}^{K_1}[f(E,K)-f(E,0)]d\ \ln K\ . \qquad (2.11)$$

$A(E)$ is a good approximation for $A_1(E)$ for large speeds of the incoming particle, because then K_m is much smaller than K_1 and the integral from 0 to K_m over $f(E,K)-f(E,0)$ is very small, while the maximum value of the momentum transfer $K_M=2v$ is much larger than the value $K_p\approx E^{1/2}$, where the function $f(E,K)$ has its maximum, and the integral over $f(E,K)$ from K_M to ∞ is small (see Figs. 3 and 4 below). At energy losses just below K_M^2, $A(E)$ defined by Eq. (2.11) is to be used; however, for $E>K_M^2$, $A(E)$ must be set equal to zero. Thus the integrals of Eq. (2.11) must be calculated only once (see Sec. III.B.). The replacement of $A_1(E)$ by $A(E)$ and the setting of $A(E)=0$ for $E>K_M^2$ is the Bethe approximation.

By combining Eqs. (2.9) and (2.11), the collision cross section for longitudinal excitations is approximated well by

$$\sigma_l(E)=E\rho(E)2Z\left[f(E,0)\ln\frac{vK_1}{E}+A(E)\right]; \qquad (2.12)$$

the dependence on speed v appears only in the Rutherford term $\rho(E)$ and in the logarithmic term, but not in $A(E)$. A different value of K_1 was chosen for each atomic shell. It may be noted that the differences between $A_1(E)$ and $A(E)$ are the "shell corrections" of stopping-power theory [Eq. (4.3)]. They are negligible for $\beta>0.25$.

D. Further details about collision cross sections

It is well known that $\sigma(E,K)$ and $\sigma(E)$ show a complex structure (Fig. 9, below) for energy losses close to the binding energies Θ of electrons, while they are quite simple for $E\gg\Theta$. It is thus useful to consider separate electron groups in the material. For silicon, K-shell electrons will not contribute to energy losses below $\Theta_K=1839$ eV, nor will L-shell electrons below $\Theta_L=99$ eV.

For the energy losses to electrons in the K- and L-shells, the atomic collision cross sections give a good approximation for the solid. For the M-shell electrons (four electrons per atom), though, the collisions produce collective excitations. The largest value of $\sigma(E,K)$ in the solid occurs at around $E=16.7$ eV for small values of K ("plasmon excitation," Fig. 7 below).

For the evaluation of Eq. (2.12) and the corresponding equations for the solid (Sec. III), the functions $f(E,K)$ and the complex dielectric function must be known. Semiempirical and theoretical approaches have been used to calculate them.

Since the contribution to $\sigma(E)$ from small K [Eq. (2.12), Fig. 9 below] is a large fraction of the total at energies E near the binding energies (clearly depending on the choice of K_1),[4] it is important to determine the dipole oscillator strength and thus the optical constants of the material accurately. These constants therefore are reviewed in Sec. II.E. The generalized oscillator strengths are dealt with in Sec. II.F, and the singly differential cross sections are derived in Sec. III. Some integral properties of $\sigma(E)$ are discussed in Sec. IV. The cross sections used here are compared with those of other papers in Sec. V.

E. Dipole oscillator strengths and optical constants

For a solid, the atomic DOS $f(E,0)$ of Eq. (2.9) is replaced by the complex dielectric function $\varepsilon(E)=\varepsilon_1(E)+i\varepsilon_2(E)$ [see Eq. (3.1)]. Because ε_1 and ε_2 are related by the Kramers-Kronig relations (Appendix A), it is only necessary to find ε_2. Values of $\varepsilon_2(E)$ were obtained from experimental and theoretical sources; $\varepsilon_2(E)$ is related simply to the optical constants n (index of refraction) and k (coefficient of extinction), and to the x-ray attenuation coefficient μ (Fano and Cooper, 1968):

$$\varepsilon_1(E)=n^2(E)-k^2(E)\ , \qquad (2.13)$$

$$\varepsilon_2(E)=2n(E)k(E)\ , \qquad (2.14)$$

$$\mu(E)=2\frac{E}{\hbar c}k(E)=2\frac{E}{\hbar c}\mathrm{Im}(\varepsilon^{1/2})\ , \qquad (2.15)$$

where $\hbar c=1.9732\times10^{-5}$ eV cm. If $\varepsilon_1\simeq1$, we have

$$\mu(E)\simeq50\,679E\varepsilon_2\ , \qquad (2.16)$$

with E in units of eV and μ in units of cm^{-1}. To get μ in Mb/atom, we divide $\mu(\mathrm{cm}^{-1})$ by $(10^{-18}N_a)=49\,940$, where N_a is the number of atoms per cm^3 (4.994×10^{22} for silicon). The relation between $\mu(E)$ and $f(E,0)$ is given in Eq. (2.20).

Values of ε_2 were determined from the sources of experimental data given in Table I. These data were supplemented by data discussed in Sec. II.E.2. In the following, the data are considered in the sequence of increasing energy. For some energy intervals, they were used as

[4] In the electron gas model (Lindhard and Winther, 1964), the distinction between distant and close collisions is much more clear-cut: "collective" or "plasmon excitations" correspond to distant collisions, all others to close collisions, and K_1 is defined exactly by the point of interception of the plasmon line with the free-electron interactions. Notice though that there are contributions to the latter for $K<K_1$.

TABLE I. Sources of data used to obtain the complex dielectric function $\varepsilon(\omega)=\varepsilon_1(\omega)+i\varepsilon_2(\omega)$. The frequency ω is represented by the corresponding energy $E=\hbar\omega$ (in eV), n is the frequency-dependent index of refraction, k is the coefficient of extinction, and μ is the absorption coefficient of electromagnetic radiation, Eqs. (2.13)–(2.16).

Range of E	Datum	Source
0–1.5	$\varepsilon_1,\varepsilon_2$	Shiles and Smith (1983)
1.5–6	$\varepsilon_1,\varepsilon_2$	Aspnes and Studna (1983)
1.8–4.7	$\varepsilon_1,\varepsilon_2$	Jellison and Modine (1983)
1.6–5.6	$\varepsilon_1,\varepsilon_2$	Viña and Cardona (1984)
6–10	$\varepsilon_1,\varepsilon_2$	Philipp (1972)
10–20	$\mathrm{Im}(-1/\varepsilon)$	See Table II
20–82.6	n,k	Hunter (1966)
60–120	μ	Tomboulian and Bedo (1956)
99–110	μ	Brown *et al.* (1977)
95–240	μ	Gähwiller and Brown (1970)
95–190	μ	Ershov and Lukirskii (1967)
277	μ	Kohlhaas and Scheiding (1968)
8000–19600	μ	Gerward (1981, 1982)
6000–25000	μ	Del Grande (1986)

found; in others, various modifications were made, as discussed below. In particular, correction factors were used to adjust calculated values to the experimental data. In addition, the correction factors were used to satisfy the sum rules discussed in Appendix B.

The tabulated data for $\varepsilon_2(E)$ from 1.5 to 6 eV (Aspnes and Studna, 1983) were used without modifications. For E from 6 to 10 eV, the values of ε_2 given by Philipp (1972) were adjusted to match the values at 6 eV. For the region above 10 eV, three different approaches were used. They are described in the next three sections.

1. Plasmon excitations

Recent measurements of energy losses between about 10 and 20 eV for fast electrons in Si were made by Stiebling and Raether (1978), Hinz and Raether (1979), Chen *et al.* (1980), and Tarrio and Schnatterly (1986a, 1986b). Theoretical values were given by Louie *et al.* (1975) and Sturm and Oliveira (1980). The data were reviewed by Hinz (1979) and Raether (1980). Fairly accurate quantitative data were available only for very small values of K; for larger values, the experimental data provided only qualitative guides for the theoretical values of $\mathrm{Im}[-1/\varepsilon(E,K)]$ discussed in Sec. II.F.3. The important parameters of the observed and calculated "energy-loss functions" $\mathrm{Im}[-1/\varepsilon(E,0)]$ are given in Table II. Hinz showed that the measured spectra can be fitted very closely by the function $\mathrm{Im}(-1/\varepsilon)$ calculated with the free-electron plasmon functions, with the parameters E_r and γ (often, the frequency ω is used in these equations; here, the energy loss $E=\hbar\omega$ is used as the independent variable):

$$\mathrm{Im}\left[\frac{-1}{\varepsilon(E,0)}\right]=\frac{E_r^2\gamma E}{(E^2-E_r^2)^2+(\gamma E)^2}\ , \tag{2.17}$$

$$\varepsilon_1(E,0)=1-\frac{E_r^2}{E^2}\frac{1}{1+(\gamma/E)^2}\ , \tag{2.18}$$

$$\varepsilon_2(E,0)=\frac{E_r^2\gamma}{E^3}\frac{1}{1+(\gamma/E)^2}\ . \tag{2.19}$$

For these functions, the maximum value of $\mathrm{Im}[-1/\varepsilon(E,0)]$ is $h=E_r/\gamma$; it is located at $E_p=E_r$; and the full width at half maximum w is equal to γ. For the comparison with the experiments, the function must be folded with the resolution function of the instrument, and the observed values of E_p, w, and h are slightly different. For the present purposes, it was assumed that the function $\mathrm{Im}[-1/\varepsilon(E,0)]$, calculated with Eq. (2.17) and with the parameters $E_r=16.7$ eV and $\gamma=3.5$ eV (from Table II), was a good approximation for the function determined in the experiments.

As outlined above, ε_1 is to be determined from ε_2 with the Kramers-Kronig relation; therefore, values of ε_2 must be found rather than values of $\mathrm{Im}(-1/\varepsilon)$. If values of ε_2 calculated with Eq. (2.19) and the parameters for the free-electron functions (Table II) are used in the Kramers-Kronig relation, we will obtain values of $\varepsilon_1(E,0)$ differing considerably from those calculated with Eq. (2.18), and thus an energy-loss function $\mathrm{Im}(-1/\varepsilon)$ differing from the desired one (i.e., the one determined experimentally). After trying some other analytic functions for ε_2, I found that Eq. (2.19), with $E_r=18.5$ eV

TABLE II. Data for plasmon excitations obtained from electron-energy-loss spectroscopy and solid-state theory. The location of the most probable energy loss E_p, the full width at half maximum w, and the maximum value h of the "loss function" $\mathrm{Im}(-1/\varepsilon)$ for Si are given. As a compromise, I have chosen $E_p=16.7$ eV, $w=3.5$ eV, and $h=4.8$ for the calculations in the text.

Authors	E_p (eV)	w (eV)	h
Stiebling and Raether (1978)	16.7	3.8	3.9
Hinz and Raether (1979)	16.9	3.2	5.1
Hinz (1979)	16.8	3.3	4.5
Chen *et al.* (1980)	16.6	3.3	
Tarrio and Schnatterly (1986a, 1986b)	16.8	3.0	5.6±0.6
Louie *et al.* (1975)	17.2	5.4	3.3
Sturm and Oliveira (1980)	17.4	3.5	4.8

and $\gamma=2.9$ eV, resulted in a calculated function $\mathrm{Im}(-1/\varepsilon)$ with $E_p=16.7$ eV, $w=3.5$ eV, and $h=4.7$ eV, in reasonable agreement with the compromise values selected in Table II, and thus differing little from the experimental function.

2. Theoretical calculation of atomic dipole oscillator strengths

Values of the dipole oscillator strength $f(E,0)$ for atoms were calculated for all electron shells by Dehmer *et al.* (1975)[5] who solved the Schrödinger equation for an independent electron model using a Hartree-Slater potential. These values were confirmed for L-shell electrons in the calculations of GOS outlined in Sec. II.F.1. For K-shell electrons, $f(E,0)$ was also calculated with the hydrogenic approximation (Walske, 1952), using an effective nuclear charge $Z_{\text{eff}}=13.5745$ according to Clementi and Raimondi (1963).

These data were used in the evaluation of experimental optical data. Within the approximation outlined by Fano and Cooper (1968), the photoabsorption coefficient (Mb/atom) is related to the calculated DOS $f(E,0)$ (eV^{-1}) by

$$\mu(E)=109.8f(E,0)\ . \tag{2.20}$$

For the L and M shells, the theoretical values of $\mu(E)$ for silicon atoms obtained with Eq. (2.20) are plotted in Figs. 1 and 2 below.

3. Evaluation of experimental optical data

Measured mass absorption coefficients μ for solid silicon for energies between 20 and 95 eV are shown in Fig. 1. Hunter's (1966) values [calculated with Eq. (2.15)], on the average, amount to only 0.65 of those of Tomboulian and Bedo (1956). This difference may be due to methods of sample preparation (Hunter, 1985). The values from the theoretical calculations of DOS for the M shell of the atom show a different curve shape. The difference must be due to the rearrangement of the electrons in the solid state. We note, in particular, that the local minimum in the theoretical $\mu(E)$ at 24 eV does not appear in the experimental μ.

It was assumed that the Hunter data were the most reliable, and they were used without any modifications from 20 to 82.6 eV. For $E\geq 82.6$ eV, the theoretical values for the atomic M-shell were used with a coefficient of proportionality determined at that energy. In order to obtain ε_2 from $\mu(E)$, it was assumed that the initial value of $\varepsilon_1(E,0)$ in Eq. (2.15) was equal to 1. In the subsequent determination of ε_1, using the Kramers-Kronig relation, ε_1 differed from 1 by no more than 2% for $E>82.6$ eV; the initial approximation therefore was adequate.

[5]Dr. Saxon kindly gave me tables of DOS.

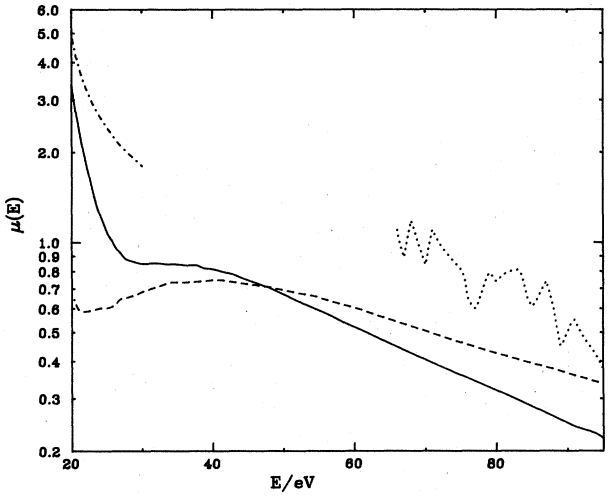

FIG. 1. X-ray absorption coefficient $\mu(E)$ (Mb/atom) as a function of photon energy $E=\hbar\omega$ for $20<E<90$ eV. The dashed line represents the theoretical data for silicon atoms of Dehmer *et al.* [1975; see also (Eq. (2.20)]. Measurements of the attenuation coefficient for solid silicon by Hunter [1966; see also (Eq. (2.15)] are represented by the solid line; those by Tomboulian and Bedo (1956), by the dotted line. Values given by Philipp (1972) are represented by the chained line. Note that the minimum for atoms ("Cooper minimum"; McGuire, 1986) at 24 eV does not appear for the solid.

For the energy range from 90 to 300 eV, calculated and measured mass absorption coefficients are shown in Fig. 2. The theoretical L-shell data were added to the M-shell data to obtain the theoretical values shown. For all the measured data, problems with surface layers were encountered. This may explain the large differences seen

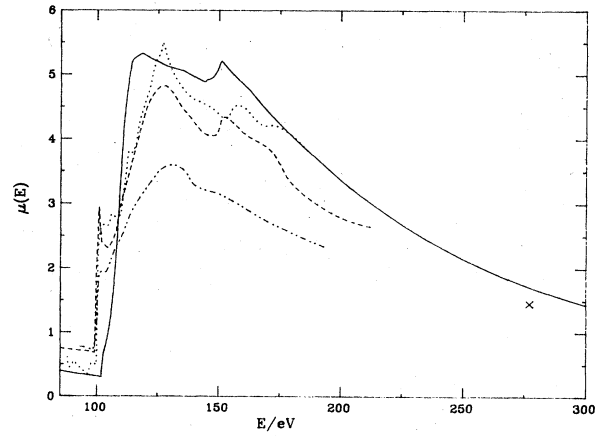

FIG. 2. X-ray absorption coefficient μ (Mb/atom) as a function of photon energy for $80<E<300$ eV. The solid line represents values obtained from theoretical dipole oscillator strengths for atomic silicon (Dehmer *et al.*, 1975). The dotted line represents the measurements of Tomboulian and Bedo (1956); the dashed line, those of Gähwiller and Brown (1970; for 99–110 eV, the data by Brown *et al.*, 1977, were used); and the chained line, those of Ershov and Lukirskii (1966). The single point at 277 eV is from Kohlhaas and Scheiding (1969).

in the figure. For 103–200 eV, the experimental values generally are less than theoretical values. The theoretical function calculated by Ritsko *et al.* (1974) had been normalized to the Gähwiller and Brown (1970) data and therefore did not provide independent information. Its shape agreed with these data. No measurements have been made for energies between 277 eV and 6 keV.

The final adjusted data for ε_2 for $E > 100$ eV were determined, using Eq. (2.16), as follows: For E from 100 to 110 eV, the experimental data for $\mu(E)$ of Brown *et al.* (1977) were used. For $E > 110$ eV, the theoretical values—multiplied with correction factors varying with energy, and chosen to approximate the experimental data and to satisfy the sum rules—were used. For 110–220 eV, the factor was 0.85, giving a function lying near the mean experimental values. Consequently, it was necessary to increase the theoretical values of $\mu(E)$ for $E > 220$ eV in order to compensate for the reduction at the lower energies [this is similar to the corrections made by Shiles *et al.* (1980) for aluminum]. Specifically, between 220 and 300 eV, a factor linearly increasing from 0.85 to 1.15 was used; for $E > 300$ eV, the theoretical values were multiplied by 1.15.

For $E > 1839$ eV, the K-shell contribution to DOS calculated with the hydrogenic approximation (Walske, 1952) was added to the M- and L-shell functions. Since the modifications made below $E = 1839$ eV were insufficient to fulfill the sum rules, the calculated values above this energy were multiplied by a factor 1.07. With these factors, the sum rules were satisfied; in addition, the I value defined by Eq. (B4) was equal to the one found experimentally (Tschalär and Bichsel, 1968). Measurements of $\mu(E)$ for $E > 6$ keV were reviewed, for example, by Gerward (1981, 1982). They agree within a few percent with the values calculated above. Clearly it is necessary to assume an uncertainty of at least $\pm 10\%$ for the values of ε_2 for $E > 20$ eV.

Besides the factors used to modify the calculated values of $\mu(E)$ given above, the energies (i.e., 220 and 300 eV given above) at which various factors changed were free parameters, too. Including the parameters used for the plasmon function, the calculation contains 12 adjustable parameters. Because the parameters apply to widely different energy regions, they are not strongly interdependent.

The full function $\varepsilon_2(E)$ was used to calculate $\varepsilon_1(E)$ with the Kramers-Kronig relation (Appendix A), and values of n, k, $\mathrm{Im}(-1/\varepsilon)$, and μ were calculated with Eqs. (2.13)–(2.15) and compared with experimental data. Values of n and k agreed with Hunter's data to within a few percent. Values of μ at 1839 eV were about 5% above the values given by Veigele (1973) and 13% above those of Storm and Israel (1970). This is reasonable, considering that for aluminum, where experimental data were available, Shiles *et al.* (1980) found values 12% above Veigele's and 17% above Storm's at 1560 eV. Values of $\mu(E)$ at 6–9 keV were 4% above those measured by Gerward (1981, 1982) and by Del Grande (1986). At 17.5–25 keV, the values agree to better than 1% with these measurements.

Calculations of the reflectance R with the data for ε determined here agreed with those given by Philipp (1972) to better than 10% for $7 \leq E/\mathrm{eV} \leq 15$. It must also be noted that the Aspnes and Studna (1983) data for ε_1 agree closely with those of Jellison and Modine (1983) except at 3.3 and 4.5 eV, where the differences of the order of 10% occur. These differences have a very minor influence for present purposes.

While Shiles *et al.* (1980) were able to determine I for aluminum from the experimental data, this was not possible for silicon because no measurements of x-ray absorption have been made for 277 eV $< E <$ 6 keV. Indeed, the experimental value (Tschalär and Bichsel, 1968) was used to adjust the parameters.

F. Generalized oscillator strengths

For small and intermediate energy losses, complete sets of values of GOS for longitudinal excitations were calculated for all three shells. The largest contribution came from the L shells; those from the K and M shells were smaller. For excitation energies much larger than the binding energy Θ of the electrons in a given electron shell of an atom, the GOS $f(E,K)$ has a pronounced maximum located near $(Ka_0)^2 = E$ (E in Ry, a_0 = Bohr radius, see Fig. 3 and, below, Fig. 7). For E near Θ, though, $f(E,K)$ changes little for small values of Ka_0 and decreases rapidly for $(Ka_0)^2 > E$ (Fig. 4). A general impression of the location of the maximum values of GOS in the (E,K) plane and the width of $f(E,K)$ for K-shell electrons can be obtained from Fig. 5. The functions are similar for other shells. For present purposes, all values of generalized oscillator strength were calculated with theoretical functions. Experimental values were available only for plasmon excitations for energy losses between 10 and 20 eV. Details for each shell are given next.

1. L shell

The calculation of generalized oscillator strength $f(E,K,l,l')$ was based on the theory presented by Manson (1972), using an independent electron model; l indicates the angular momentum of the ground state, l' that of the excited state. It was necessary to calculate values for the ground state of each subshell and for all continuum states with all values of the final-state angular momentum l'. The excitation energy, equal to the energy loss, is E (note that the energy given to the electron in an ionization process is equal to $E - \Theta$); the momentum transfer in the collision is K. The principal quantum number is not indicated.

The numerical calculation of $f(E,K,l,l')$ consisted of (Manson, 1972) (1) selection of a suitable grid for the radial distance from the nucleus and interpolation of the

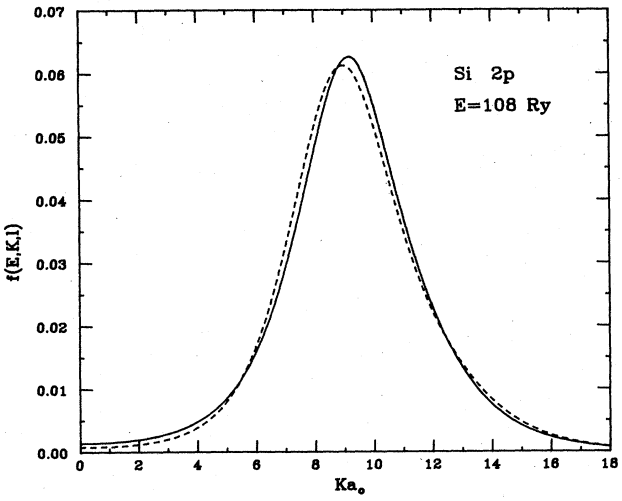

FIG. 3. Generalized oscillator strength $f(E,K,l)$, in Ry^{-1}, for longitudinal excitations for the $2p$ shell ($l=1$, $\theta=7.954$ Ry) of silicon atoms, for an energy loss $E=108$ Ry (solid line). The abscissa represent the momentum transfer K (in atomic units) occurring in the collision. The sum over all values of the final-state angular momentum l' has been calculated [Eq. (2.21)]. For comparison, the function calculated with the hydrogenic approximation is also given (dashed line). Note that for $Ka_0<1$, the values differ very little from the DOS $f(E,0,l)$; thus the second integral in Eq. (2.11) will be very small. The maximum value of $f(E,K,l)$ is located at $K_p a_0=9.2$, and contributions for $Ka_0>17.5$ are very small. For 30-MeV protons, $K_M a_0\approx 70$; therefore, replacing $A_1(E)$ of Eq. (2.10) by $A(E)$ of Eq. (2.11) causes a very small error. At this energy loss ($E=1470$ eV), GOS provides the largest part of the collision cross section, Eq. (3.8): for 1-GeV electrons, the contributions are σ_l, 4%; σ_t, 15%; and $\sigma_u(E)$, 81%.

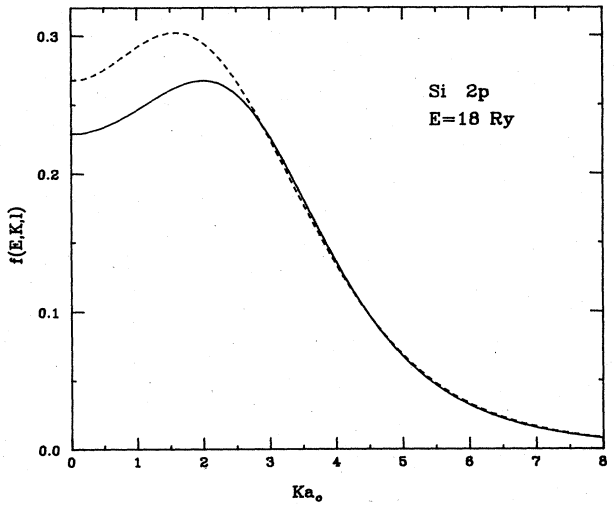

FIG. 4. Generalized ocillator strength $f(E,K,l)$ for the $2p$ shell of silicon atoms, for an energy loss $E=18$ Ry (solid line). The abscissa represents the momentum transfer K (in atomic units) occurring in the collision. The sum over all values of the final-state angular momentum l' has been calculated. The function obtained from the hydrogenic approximation is given by the dashed line. Here, the contributions for 1-GeV electrons from the three parts of Eq. (3.8) are almost evenly divided: σ_l [Eq. (3.1)], 40%; σ_t [Eq. (3.2)], 26%; σ_u [Eq. (3.3)], 34%.

potential and of the ground-state wave function from Herman-Skilman (1963) tables for this grid, (2) selection of values of E and l', (3) calculation of the continuum-state wave function for these values of E and l' by numerical integration of the Schrödinger equation, (4) calculation of the radial matrix elements for several values of K, (5) calculation of $f(E,K,l,l')$.

Values were calculated for excitation energies $0.1+\Theta\le E/\mathrm{Ry}\le 550+\Theta$, momentum transfers $0\le Ka_0\le 35$ and values of the final-state angular momentum $0\le l'\le l'_M$ for $2s$ ($l=0$) and $2p$ ($l=1$) ground states. l'_M was small for small energies and up to 24 for large energies. Since the sum over all l' is needed in the calculations of $\sigma(E)$,

$$f(E,K,l)=\sum_{l'=0}^{\infty} f(E,K,l,l')\ , \tag{2.21}$$

it is necessary to determine values for $l'>l'_M$. In Fig. 6, $f(E,K,l,l')$ is shown as a function of l' for $2p$ electrons, $E=48$ Ry, and three values of K. It appears that an exponential function will closely approximate GOS for large values of l': $f(E,K,l,l')=C(E,K,l)\exp[-\alpha(E,K,l)l']$. This function has been used to extend the sum in

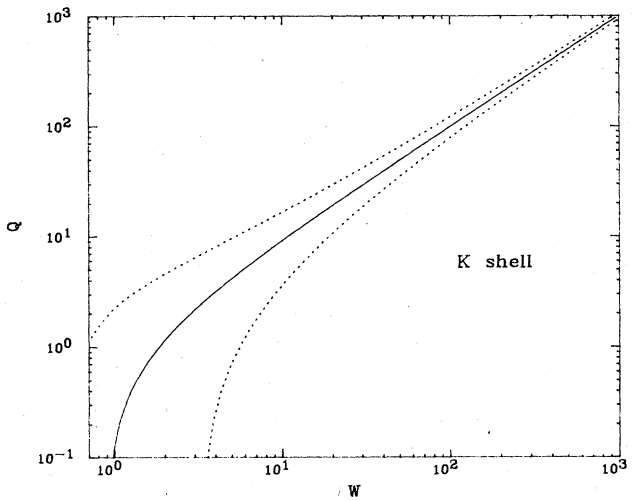

FIG. 5. Contour map of generalized oscillator strength $f(W,Q)$ for K-shell electrons. $f(W,Q)$ is calculated in the hydrogenic approximation and is valid for all atoms, with W, the excitation energy E in units of $E_0=\mathrm{Ry}\times Z_{\mathrm{eff}}^2$, and Q, the square of the momentum transfer K, divided by twice the electron mass, again in units of E_0 (Walske, 1952). The solid line represents the locus of the maximum value of $f(W,Q)$. Shown as dotted lines are the values of W where, for a constant value of Q, $f(W,Q)$ is one-tenth of the maximum value. Excitations to discrete energy levels are not shown. For large values of Q or W, the GOS is quite narrow, and the maximum value is located at $W=Q$. Photographs of a three-dimensional model of this figure are shown in Fig. 10 of Inokuti (1971). For $2p$ electrons in silicon, for two selected energies, $f(E,K)$ along a vertical line (i.e., $E=$const) is shown in Figs. 3 and 4.

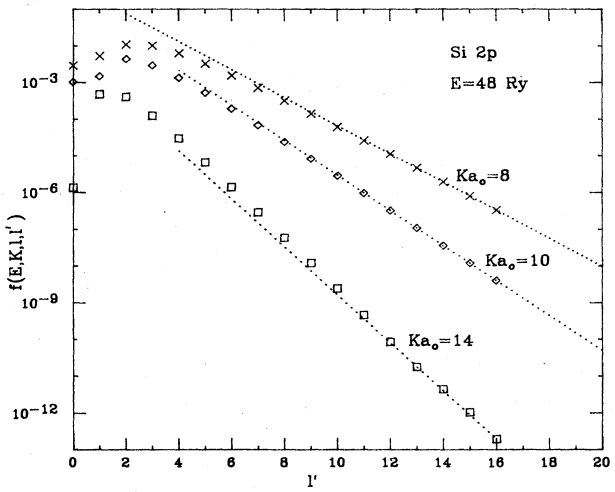

FIG. 6. Generalized oscillator strength $f(E,K,l,l')$ for $2p$ electrons in silicon as a function of l', the angular momentum of the final-state wave function. The excitation energy is $E=48$ Ry. GOS is shown for $Ka_0=8$ (crosses), 10 (diamonds), and 14 (squares). For sufficiently large l', an exponential function $C\exp(-\alpha l')$ provides a very good approximation for $f(E,K,l')$ [below Eq. (2.21)]. For $Ka_0=8$, the average deviation between the analytic function and the tabulated values amounts to $\pm 0.2\%$ for $l' \geq 13$ (for $l' < 13$, the tabulated values are systematically lower). For $Ka_0=10$, the average deviation is $\pm 0.4\%$. However, for $Ka_0=14$, for $l' > 11$, the differences are as much as $\pm 15\%$. The contribution for $l' > 16$ to the sum of Eq. (2.21) amounts to less than 0.1% for all three values of Ka_0.

Eq. (2.21) to infinity.

A comment may be made here about the calculations of GOS for Al by McGuire *et al.* (1982). They calculated values only for $l' \leq 12$. Thus it is interesting to consider the residual contribution for the calculation in Eq. (2.21). For silicon (which is quite similar to Al in the inner shells), the ratio of the sum from $l'=13$ to ∞ to the total sum is 8.5% for 300 Ry, and it is 21% at 500 Ry. Therefore the stopping numbers B (Sec. IV) calculated by these authors will be too small, especially at high particle speeds.

The accuracy of the numerical calculations was checked in various ways. For example, radial integrals for the matrix elements were calculated for given intervals Δr in r and also with intervals $2\Delta r$. Differences between these two results usually amounted to much less than 0.1%. Only when $f(E,K,l,l')$ was small (if, e.g., for some values of K the radial matrix element changes sign) were larger differences seen. A further indication of numerical errors can be seen in Fig. 6: most likely, the differences between the analytic functions and the numerical values are due to numerical errors of the latter. For the sum, $f(E,K,l)$, these errors contribute very little: for $K=10.2$, the contribution for $l' > 13$ to the sum amounts to only 0.01% of the total. Further estimates of errors will be given in Sec. III.C. Examples of the total GOS, $f(E,K,l)$, for $2p$ electrons are given in Figs. 3 and 4. For comparison, functions calculated with the hydrogenic approximation (Choi *et al.*, 1973) are also given.

2. *K* shell

The calculations with Manson's program are expensive. For K-shell electrons, they give values of $f(E,K)$, which for most energy losses E differ by less than 3% from values calculated with the screened hydrogenic approximation (Walske, 1952; Inokuti, 1971). Therefore I have used it for the calculation of GOS (Fig. 5). The value of the effective charge, $Z_K=13.5745$ given by Clementi and Raimondi (1963), was used, and the smallest excitation energy was assumed to be the binding energy $\Theta_K=1839$ eV (Bearden and Burr, 1967).

3. *M* shell

Tung *et al.* (1976) gave a model for the interaction of electrons with the valence band of insulators and derived an analytic equation for the imaginary part of the dielectric function. I have used this equation to calculate $\varepsilon_2(E,K)$. The parameters needed were obtained by calculating $\varepsilon_2(E,0)$, varying them until $\varepsilon_2(E,0)$ agreed with the values found in Sec. II.E. Then, $\varepsilon_1(E,K)$ was calculated with the Kramers-Kronig relation. In addition, the sum rules of Appendix B were used to check the results. For several values of E, $\mathrm{Im}[-1/\varepsilon(E,K)]$ is given as a function of K in Fig. 7. It is seen that the function changes quite rapidly for small Ka_0. Therefore, for $E < 100$ eV, $K_1=0.025$ was used in the calculations with Eq. (2.9). The location in the E-K plane of the maximum of $\mathrm{Im}[-1/\varepsilon(E,K)]$ ("bulk-plasmon dispersion") calculat-

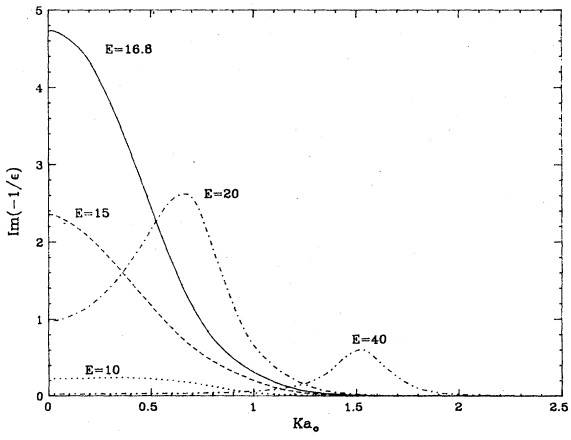

FIG. 7. "Loss function" $\mathrm{Im}[-1/\varepsilon(E,K)]$ as a function of momentum transfer K (in atomic units) and energy loss E (in eV) near the plasmon peak (16.7 eV). The functions were calculated with the model given by Tung *et al.* (1976). For energy losses below and slightly above the plasmon energy, the function varies little for $Ka_0 < 0.1$, then drops quite quickly. For larger energies, the function begins to show a pronounced maximum at $(Ka_0)^2 \approx E/\mathrm{Ry}$. For energy losses less than 100 eV, $K_1 a_0=0.025$ was used for Eqs. (2.9) and (2.11).

ed with this function is in reasonable agreement with the data given by Stiebling and Raether (1978) and Chen *et al.* (1980); the full width at half maximum increases with increasing K, as observed in the experiments, but no quantitative data were available from the experiments.

It was found that, for $E > 100$ eV, the above function differed little from the free-electron function given by Lindhard and Winther (1964). The latter function was used for $E > 100$ eV. It may be noted that $I_f = \int \mathrm{Im}[-1/\varepsilon(E,K)]d\ \ln K$, which is equivalent to Eq. (2.11), is approximated well for $E \gg E_f$ by $I_f = \rho(E)4(1+0.8E_f/E)$, where $E_f = 12.46$ eV is the Fermi energy [see Eq. (3.4)].

4. Generalized oscillator strengths for large energy losses for all shells

For large energy losses, $f(E,K)$ is large only near the value $K^2 = E$ (Figs. 3 and 5). For $E \ll (M/m)Mc^2$, Fano (1963) approximated the longitudinal and transverse matrix elements by [Fano's Eq. (28)]

$$|F(E,\mathbf{K})|^2 \approx \frac{1+Q/2mc^2}{1+Q/mc^2}\delta(E,\mathbf{K}) , \tag{2.22}$$

$$|\boldsymbol{\beta}_t \cdot \mathbf{G}(E,K)|^2 \approx \beta_t^2 \frac{Q/2mc^2}{1+Q/mc^2}\delta(E,\mathbf{K}) , \tag{2.23}$$

where the Kronecker δ indicates that the matrix elements vanish unless the state E is an eigenstate of momentum K. In Eq. (2.23) it can be seen that for $Q \ll 2mc^2$ the transverse matrix elements will be small compared to the longitudinal ones because of the factor $Q/2mc^2$ in the numerator. With this approximation the integral in Eq. (2.11) will be equal to zero for $E > E_M$ and equal to

$$A(E) = \frac{1}{E}\left[\frac{1}{1+s} + \frac{s}{1+s} - s(1-\beta^2)\right], \quad E < E_M \tag{2.24}$$

with $s = E/2mc^2$. The first term in the large parentheses stems from the longitudinal excitations, the second and third from the transverse ones. The dependence on particle speed appears in two places: first in the term $(1-\beta^2)$ and second in the fact that the cross section is zero for E greater than the speed-dependent E_M [see Eq. (3.6)].

III. CROSS-SECTION DIFFERENTIAL IN ENERGY LOSS

To calculate straggling functions, the collision cross section $\sigma(E)$ differential in energy loss E is needed. According to the discussion in the previous section, three contributions to $\sigma(E)$ can be discerned. They are given next.

In addition to the dependence of the Rutherford cross section, Eq. (2.1), on the charge z of the particle, the collision cross section depends on higher powers of z [Bloch, 1933; Ashley *et al.*, 1972; Jackson and McCarthy, 1972; see also Eq. (4.3)]. These effects are negligible for the particle speeds under consideration here.

A. Small momentum transfers

For the longitudinal low-K excitations in a solid material, Fano (1963) gave the following equation [his Eq. (45)] for $\sigma(E)$. It replaces Eq. (2.9) for atoms (here, cgs units are used, thus $Q = K^2/2m$; furthermore, $E \ll mc^2$):

$$\sigma_l(E) = \frac{z^2e^2}{\pi v^2}\mathrm{Im}(-1/\varepsilon)\ln\frac{Q_1}{Q_m} = \frac{z^2e^2}{\pi v^2}\mathrm{Im}(-1/\varepsilon)\ln\frac{2mv^2Q_1}{E^2} , \tag{3.1}$$

where $\varepsilon = \varepsilon(E,0)$ is the complex dielectric constant for $K = 0$ as a function of energy loss E, and Q_m is given approximately by $Q_m = E^2/2mv^2$ [Fano's Eq. (18)]. Thus, to get $\sigma_l(E)$, it is simply necessary to calculate $\mathrm{Im}(-1/\varepsilon) = \varepsilon_2/(\varepsilon_1^2+\varepsilon_2^2)$ from the data described in Sec. II.E. For $E < 100$ eV, $K_1a_0 = 0.025$ was used ($Q_1 = 6.25\times10^{-4}$ Ry); for $E > 100$ eV, $K_1a_0 = 1$ was used ($Q_1 = 1$ Ry).

For the transverse excitations, the cross section is given by Fano's Eq. (47), which replaces Eq. (2.6a):

$$\sigma_t(E) = \frac{z^2e^2}{\pi v^2}\left[\frac{\varepsilon_2}{\varepsilon^2}\ln[(1-\beta^2\varepsilon_1)^2+\beta^4\varepsilon_2^2]^{-1/2} + \left[\beta^2 - \frac{\varepsilon_1}{\varepsilon^2}\right]\arctan\frac{\beta^2\varepsilon_2}{1-\beta^2\varepsilon_1}\right] . \tag{3.2}$$

In the calculation of $\sigma(E)$, the contributions $\sigma_l(E)$ and both parts of $\sigma_t(E)$ were calculated separately in order to assess their relative importance. For $E > 4000$ eV (twice the binding energy of the K shell), σ_l and σ_t decrease rapidly with increasing E (approximately proportional to E^{-4}, according to the numerical data). For energy losses E where ε_1 is almost equal to 1 and $\varepsilon_2 \ll 1$, problems may arise in the evaluation of the ln term in Eq. (3.2) with a computer with 32-bit words.

B. Large momentum transfers

For longitudinal excitations, the function $A(E)$ of Eq. (2.11) was calculated numerically for all electron shells with the GOS described in Sec. II.F. The function for $2p$ electrons of silicon is shown in Fig. 8. For comparison, the corresponding function calculated with the hydrogenic approximation is also given. It is seen that the Hartree-Slater results are approximated by the hydrogenic calculations for $E > 300$ Ry to better than 1%. The collision cross section for large momentum transfers K is [Eq. (2.12)]

$$\sigma_u(E) = 2Z\rho(E)\sum_l EA_l(E) , \tag{3.3}$$

where the sum is over all subshells l. For all electron

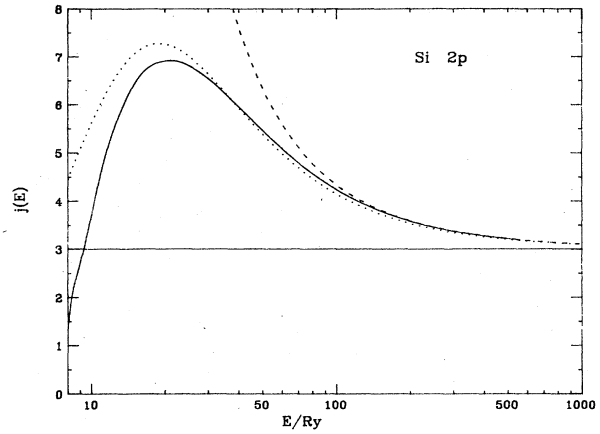

FIG. 8. Function $A(E)$ of Eq. (2.11) for the longitudinal excitation of electrons in close collisions. $A(E)$ is used to obtain the differential collision cross section $\sigma_u(E)$ of Eq. (3.3). $A(E)$ was calculated with the Hartree-Slater (solid line) and the hydrogenic approximation (dotted line) for $2p$ electrons in silicon as a function of energy loss E. The function $j(E)=6EA(E)$ is shown. The approximation function of Eq. (3.4) is also shown as the dashed line. The Rutherford cross section, Eq. (2.1), multiplied by $(2l+1)\beta^2E^2/k$, is represented by the horizontal line at $j(E)=3$.

shells, for energy losses E much larger than the binding energies Θ of the electrons, I have found empirically that the function $A(E)$ of Eq. (2.11) can be approximated by

$$A_l(E)=\frac{Z_l}{ZE}\left[1+\frac{d_1}{E}+\frac{d_2}{E^2}\right], \tag{3.4}$$

where Z_l is the number of electrons in the subshell. The coefficients used for the present calculations are given in Table III. This equation corresponds to that derived by Inokuti (1971) from the binary-encounter theory [Inokuti's Eq. (4.87), where d_1 was equal to $4\Theta/3$]. For the $2s$ and $2p$ shells, calculations of $A(E)$ were made up to $E_1=558$ Ry$\approx 69\Theta$. For $E>200$ Ry, the deviation between the integral of Eq. (2.11) and the approximation function of Eq. (3.4) was less than 0.1%. This leads me to conclude that no serious errors occurred in the numerical calculations of GOS; in particular, the intervals used in the radial integrations of GOS and in the momentum transfer K were small enough to cause no problem in the numerical integrations. Similar agreement was found for the K shell.

TABLE III. Coefficients Z_l, d_1, and d_2 for the asymptotic equation of $A(E)$ [Eq. (3.4)]. The equation is valid for energy losses E greater than E_a. ζ is Clementi and Raimondi's (1963) orbital charge coefficient, and the effective nuclear charge is $Z_{\text{eff}}=n\zeta$, where n is the principal quantum number. Then, $d_1=(\frac{4}{3})Z_{\text{eff}}^2$ Ry$/n^2=(\frac{4}{3})\zeta^2$ Ry for K- and L-shell electrons. E_a, d_2 for all shells and d_1 for the M shell were determined from a least-squares fit to values of $A(E)$ calculated with Eq. (2.11).

Shell	Z_l	ζ	E_a (eV)	d_1 (eV)	d_2 (eV^2)
K	2	13.57	20 000	3340	0
L					
$2s$	2	4.51	4 000	369	1.94×10^6
$2p$	6	4.97	3 000	448	2.07×10^5
M	4	1.53	150	9.4	31.2

C. Approximation for large energy losses

For arbitrarily large energy losses, Uehling (1954) gave the relativistic Rutherford cross section:

$$\rho_r(E)=\rho(E)(1-\beta^2E/E_M), \tag{3.5}$$

where

$$E_M=Mc^2\beta^2\gamma^2/[(M/2m)+(2m/M)+\gamma]. \tag{3.6}$$

These equations supersede Eq. (2.24). Further correction terms differing for particles with different spins (Uehling, 1954) can be neglected in the present application.

It appears reasonable to keep the terms d_1/E and d_2/E^2 of Eq. (3.4) for large E. The functions of Eqs. (3.3)–(3.5) are thus combined into[6]

$$\sigma_u(E)=\rho(E)\left[1-\beta^2\frac{E}{E_M}\right]\sum_l Z_l\left[1+\frac{d_1}{E}+\frac{d_2}{E^2}\right]. \tag{3.7}$$

A more detailed study of the cross section for large energy losses to bound electrons can be found in Anholt (1979) and Davidović *et al.* (1978). The relativistic correction terms given there are small for the energy losses used in the present theory (Secs. VIII and X).

D. Total singly differential cross section

In order to obtain the total cross section, the functions for small and large momentum transfer, Eqs. (3.1)–(3.3), are added, resulting in

$$\sigma(E)=\sigma_l(E)+\sigma_t(E)+\sigma_u(E). \tag{3.8}$$

At $E=30$ keV, the contribution from $\sigma_l(E)$ and $\sigma_t(E)$ is

[6]This is the approach used in earlier work (Bichsel, 1985a; Bichsel and Yu, 1972). Another approach would be to apply the terms d_1/E and d_2/E^2 of Eq. (3.4) only to the longitudinal excitations. Equation (3.7) would then be replaced by

$$\sigma_u(E)=\rho(E)Z\left[1-\beta^2\frac{E}{E_M}\right]+\rho(E)\sum_l Z_l\frac{1}{1+s}\frac{d_1}{E},$$

where d_2 has been neglected. This change is of little consequence for the calculations of Sec. VIII to X and of δ_2 with Eq. (4.5); for example, ${}_u\delta_2=2100$ keV^2/cm for the example below Eq. (4.7), but it does change substantially the values of ${}_g\delta_2$, calculated with the equivalent of Eq. (4.7), for $E_1>2mc^2$: ${}_g\delta_2=70$ keV^2/cm, much less than the result ${}_g\delta_2=1170$ keV^2/cm^2 with Eq. (4.7). For the present study, the exact result for δ_2 is unimportant (see Appendix G).

only 1%. For energy losses greater than 30 keV, $\sigma_u(E)$ of Eq. (3.3) is replaced by that of Eq. (3.7). At $E=E_M$, $\sigma(E)$ drops to zero abruptly. An example of the complete collision cross section $\sigma(E)$ as well as the individual terms of Eq. (3.8) is shown in Fig. 9. For electrons and positrons, the cross section for large energy losses are given in Eqs. (9) and (10) of Uehling (1954); but the deviations from the Rutherford cross section, Eq. (3.5), are extremely small for all but two of the experiments in Table IX below ($T=0.98$ MeV, where the deviations are still small).

E. Errors

The data obtained for the differential collision cross section $\sigma(E)$ appear to be adequate for present purposes (Table VII, below). In particular, for the most important region in the DOS extending from 0 to 300 eV, the errors in the values of $\mathrm{Im}(-1/\varepsilon)$ are probably less than 10%. For $E>300$ eV, the errors may be as much as 20%. Further optical measurements would be highly desirable for $6<E/\mathrm{eV}<3000$, especially to determine the I value independently of measurements of stopping power.

An undesirable aspect of the data is the following: for small momentum transfers (i.e., $Ka_0<1$), experimental data of DOS were used. For the L shell, for $Ka_0>1$, the theoretical values of GOS were used. They differ, at $Ka_0=1$, by as much as 15% from the experimental values. A further study of this problem would be desirable.

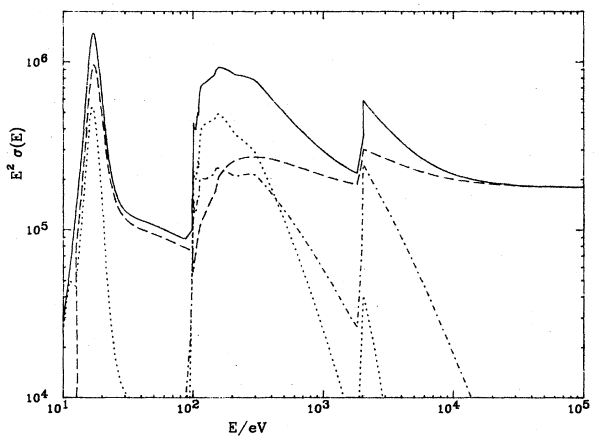

FIG. 9. Total differential collision cross section ("energy-loss spectrum") $\sigma(E)$ of Eq. (3.8) for energy loss E in a single collision of pions with momentum of 45 GeV/c in solid silicon (solid line). In order to show the structure of $\sigma(E)$ more clearly, the function $E^2\sigma(E)N_a$ (in eV/cm) is plotted. Maxima are clearly seen at 17,200, and 1900 eV. They are associated with the M, L, and K shells of silicon and are determined mainly by the optical-absorption coefficients of the material. These optical data therefore must be known quite well (Sec. II.E). For $E>50$ keV, the cross section for each shell is proportional to the number of electrons in the shell; the function decreases as $(1-\beta^2E/E_M)$ [Eq. (3.5)] and drops to zero at $E=E_M=32$ GeV. The moments of $\sigma(E)$ are $M_0=38\,200$ cm^{-1}, the collision cross section (number of collisions per cm); $M_1=5.33$ MeV/cm, the stopping power; $M_2=2.8\times10^9$ MeV^2/cm, related to the width of the straggling curve; and $\delta_2=3370$ keV^2/cm. The mean energy loss per collision is $\langle E\rangle=M_1/M_0=139$ eV. The separate contributions σ_l [dotted line, Eq. (3.1)], σ_t [chained line, Eq. (3.2)], and σ_u [dashed line, Eq. (3.3)] multiplied with N_aE^2 are also shown. The nonrelativistic Rutherford cross section would be represented by a horizontal line at 1.8×10^5.

IV. INTEGRALS OVER $\sigma(E)$

In most references, integrals of $\sigma(E)$ over the energy loss E were used [e.g., collision cross sections: Anholt (1979); stopping power: Tschalär and Bichsel (1968); Ahlen (1980); density effect: Sternheimer and Peierls (1971); straggling functions: Hancock *et al.* (1983)]. For this section, integrals over $\sigma(E)$ were calculated and compared with other results. Numerical calculations and integrations of $\sigma(E)$ were made for $E<1.4$ MeV with Eq. (3.8); the residual integrations for $E>1.4$ MeV to E_M were obtained analytically, using Eq. (3.7).

A. Moments

One set of integrals is defined by the moments

$$M_\nu=N_a\int_0^\infty E^\nu\sigma(E)dE,\quad \nu=0,1,2,\ldots. \tag{4.1}$$

We note that $\sigma(E)=0$ for $E>E_M$ in the present formulation, Eqs. (3.7) and (3.8).

The moment M_0 determines the average number n of collisions of the particles in the absorber by $n=tM_0$, where t is the thickness of the absorber; n is the major determinant factor for the most probable energy loss Δ_p.

B. Stopping power M_1 and stopping number B

The mean total energy loss $\langle\Delta\rangle$ is used in the Shulek function (Appendix D). It is given by the first moment, usually called the stopping power: $\langle\Delta\rangle=tM_1$. In the present application, $\langle\Delta\rangle$ is usually much larger than Δ_p and is not relevant for straggling functions (Figs. 18–21 below). A check of the present data is given by the values of M_1, calculated with Eq. (4.1), compared to stopping-power values, obtained from the Bethe theory, for particles of kinetic energy T (see e.g., Bichsel and Porter, 1982) given by (in units of MeV cm^2/g)

$$\frac{dT}{dt}=\frac{0.307\,08}{\beta^2}\frac{z^2Z}{A}B\ , \tag{4.2}$$

with the stopping number B (called L by Lindhard and Winther, 1964, and others) for ions heavier than electrons:

$$2B=\ln\frac{2mc^2\beta^2\gamma^2E_M}{I^2}-2\beta^2-2\frac{C(\beta)}{Z}-\delta(\beta)+2[zL_1(\beta)+L_2(\beta)]\,,$$
$$\beta^2\gamma^2=\left[\frac{T}{Mc^2}+1\right]^2-1,\quad \beta^2=\frac{T}{Mc^2}\left[2+\frac{T}{Mc^2}\right]\,, \tag{4.3}$$

where E_M is given in Eq. (3.6), $I=174$ eV is the mean excitation energy [Eq. (B4)], $C(\beta)$ represents the shell corrections, $\delta(\beta)$ the density effect, $L_1(\beta)$ the Barkas effect, and $L_2(\beta)$ the Bloch correction term. For the present use, $C(\beta)$, L_1, and L_2 are negligibly small, and $\delta(\beta)$ is discussed in Sec. IV.E. It may be noted that for the calculation of stopping power with Eq. (4.1) with the $\sigma(E)$ of Eq. (3.8), no density corrections need be introduced for the numerical calculations, because the correct function, Eq. (3.2), is used for the transverse excitations.

For very large speeds, $\gamma\gg100$, it is preferable to use $\delta(\beta)$ of Eq. (4.9), as suggested by Fano (1963, p. 21, footnote 18), resulting in

$$2B=\ln\frac{2mc^2E_M}{(\hbar\omega_p)^2}-1-2\frac{C(1)}{Z}=19.777+\ln(E_M/\text{MeV})\,, \tag{4.4}$$

where $\hbar\omega_p=31.048$ eV is the plasma frequency for silicon, and $C(1)/Z\approx0.0021$ is the asymptotic value of the shell corrections. Relativistic correction terms of order z^3 and higher were neglected (Jackson and McCarthy, 1972). For $\gamma=100$, Eq. (4.4) gives a value of B greater by 0.4% than Eq. (4.3).

C. Second moment and δ_2

For particles with $\beta^2\ll1$, M_2 is related to the width of the straggling functions. For relativistic particles, M_2 seems to be quite useless. For the Shulek function, the important quantity is the difference δ_2 between M_2 and M_2',

$$\delta_2=M_2-M_2'\,, \tag{4.5}$$

where M_2' is the moment for the Rutherford collision cross section, Eq. (3.5),

$$M_2'=ZN_a\int_0^{E_M}E^2\rho(E)(1-\beta^2E/E_M)dE=ZN_aE_M\frac{k}{\beta^2}\left[1-\frac{\beta^2}{2}\right] \tag{4.6}$$

(Bichsel, 1972). For energy losses less than E_1, M_2 is obtained by numerical integration of Eq. (3.8). For $E>E_1$, an analytic integral can be obtained for δ_2 from Eq. (3.7), neglecting d_2,

$${}_g\delta_2=ZN_a\int_{E_1}^{E_M}E^2\rho(E)\left[1-\beta^2\frac{E}{E_M}\right]\frac{d_1}{E}dE=N_a\frac{k}{\beta^2}Z\langle d_1\rangle\left[\ln\frac{E_M}{E_1}-\beta^2\left[1-\frac{E_1}{E_M}\right]\right]\,, \tag{4.7}$$

where $\langle d_1\rangle$ is the average value of d_1 for the shells, $\langle d_1\rangle=728$ eV for silicon (Table III). The total value of δ_2 is the sum of the numerical integral over $\sigma(E)$ of Eq. (3.8) and the integral of Eq. (4.7).

Example: 45 GeV/c pions, $E_M=31.6$ GeV, $N_akZ=178.3$ keV/cm. From numerical calculation with $\sigma(E)$ for energies E below $E_1=1.4$ MeV, a value ${}_u\delta_2=2100$ keV^2/cm was obtained. The contribution from E_1 to E_M then is ${}_g\delta_2=1170$ keV^2/cm, for a total value $\delta_2=3270$ keV^2/cm. Because δ_2 is the difference of two large numbers, its value has an uncertainty of a few percent (footnote 6).

In the theory of Shulek *et al.* (1967), all deviations from the relativistic Rutherford cross section [Eq. (3.5), or Eq. (2) in Uehling, 1954] should be included in the calculation of δ_2. In particular, this includes the expressions of Eqs. (3) and (4) in Uehling for particles with spin greater than zero; for electrons and positrons, Eqs. (9) and (10) in Uehling should be used for $\sigma(E)$, but then δ_2 will be very large, and the considerations of Appendix G are highly relevant. For present applications concerning electrons and positrons, Figs. 11 and 12 below, numerical values of δ_2 were calculated with $E_1=1.4$ MeV as the upper limit of the integral. These values will be smaller than those extending to E_M. Since for thicker detectors ionization by the bremsstrahlung generated in the detector itself would become increasingly important (Appendix I), all theories would have to be corrected for this effect, and δ_2 would not be a meaningful parameter. Further considerations about values of δ_2 are given in Appendix G. Approximations to δ_2 used in earlier studies are described in Appendix H.

D. Results for moments

It is instructive to consider the contribution to the moments as a function of energy loss E. The integrals M_0 and M_1 are given as a function of the upper limit E of the integral, Eq. (4.1), in Fig. 10. Clearly, the detailed structure of $\sigma(E)$ near the plasmon peak (≈17 eV) is important to M_0, while for M_1 the L-shell excitations ($E>100$ eV) are important. For heavy charged particles (protons, pions), M_1 calculated numerically with Eq. (4.1) agrees with stopping powers calculated from the Bethe theory [i.e., Eq. (4.2)] to better than 0.3%. For electrons with kinetic energies between 300 keV and 1 GeV, values of M_1 calculated with the present data agree to better than 0.5% with values presented in ICRU (1984). This agreement does not prove very much about the accuracy of $\sigma(E)$, since the DOS has been adjusted to give the I value used in Eq. (4.3).

No independent data are available for the total collision cross section M_0 (Inokuti, 1971) and the second moment M_2. Values of $\delta_2(E)$ are given in Fig. 10. The most important contribution to δ_2 comes from the K shell. As shown in Appendix G, δ_2 calculated to E_M is

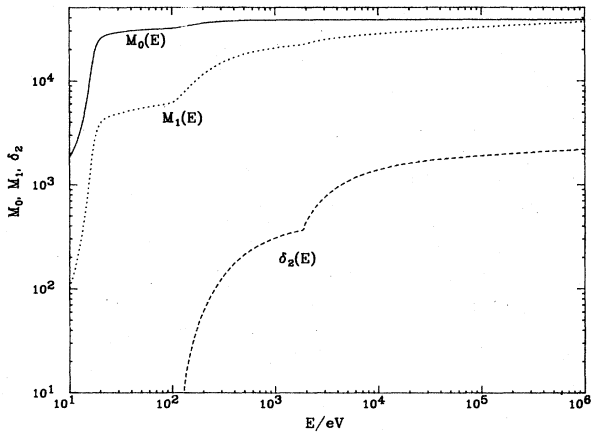

FIG. 10. Moments M_0 (solid line) and M_1 (dotted line), Eq. (4.1), as a function of energy loss E for 45-GeV/c pions. M_0 reaches 99.9% of its full value of 38 400 cm^{-1} at $E=850$ eV; one-half of all collisions occur for $E<19$ eV, and 80% occur for $E<50$ eV. The first moment M_1 reaches one-half of its full value at $E=5$ keV and 70% at 1350 keV. The function δ_2 of Eq. (4.5) is also given. It is quite small for $E<\Theta_K=1839$ eV, the binding energy of K-shell electrons. At $E=1.82$ keV, $\delta_2=368$ keV^2/cm; its value at $E_M=32$ GeV [Eq. (3.6)] is $\delta_2=3370$ keV^2/cm. For the range of energy losses shown, M_2 reaches only 7×10^{-6} of its final value and is not shown.

not a useful quantity for most cases discussed in Secs. VIII and X.

E. Density effect δ

Fano (1963) described the density effect δ as the difference between the integral over transverse low-K excitations for very low densities [shown in Fano's Eq. (32)], i.e.,

$$-\ln(1-\beta^2)-\beta^2 , \tag{4.8}$$

and the integral over the cross section $\sigma_t(E)$ of Eq. (3.2) for materials with finite densities.

Another approach, described by Fano's Eq. (48), gives δ directly. This approach was also discussed by Inokuti and Smith (1982) and was used by them to calculate δ for Al. Calculations for silicon were performed with both of these methods. The differences between the two calculations were less than 0.3%. They were due in part to different methods used for the numerical integrations.

For $\gamma>740$, an asymptotic function for $\delta(\beta)$ was given by Sternheimer *et al.* [1982, 1984; $\hbar\omega_p=31.048$ eV, see Eq. (4.3) for γ^2]:

$$\delta(\beta)=\ln\gamma^2-\ln(I/\hbar\omega_p)^2-1$$
$$=\ln\gamma^2-4.447 . \tag{4.9}$$

For $\gamma<740$, Sternheimer gave other equations, which were used in ICRU (1984). Values of δ calculated with the three methods are given in Table IV. For electrons with kinetic energies above 2 MeV, the differences between the present calculations and the ICRU values are less than 2%; but for smaller speeds, very large differences were found, similar to those found by Inokuti and Smith for aluminum.

TABLE IV. Density correction for silicon, for electrons with kinetic energy T. Values for three different approximations are given: column 1, calculated with Fano's Eq. (48); column 2 is the difference between Eq. (4.8) and the integral over Eq. (3.2); column 3 is from ICRU (1984), or Eq. (4.9) for $T>400$ MeV. The large differences between columns 1 and 3 for the lowest energies are similar to those found by Inokuti and Smith (1982) for aluminum.

T (MeV)	1	2	3
0.2	0.0321	0.0327	0.0487
0.4	0.1017	0.1023	0.1216
1	0.322	0.323	0.342
5	1.357	1.352	1.351
10	2.216	2.209	2.239
30	3.939	3.953	4.003
100	6.145	6.174	6.179
300	8.290	8.332	8.325
1000	10.68	10.73	10.72

V. APPROXIMATIONS USED IN OTHER PAPERS

Collision cross sections have been given in many papers. Here, only those functions used in papers concerned with the calculation of straggling functions will be compared with the cross section $\sigma(E)$ of Fig. 9. The Rutherford cross section, Eq. (2.1), was used, for example, by Bohr (1948) and Landau (1944). Vavilov (1957) included the relativistic correction of Eq. (3.5), while Livingston and Bethe (1937), and later Shulek *et al.* (1966), included the binding correction term of Eq. (3.7).

The large resonance contributions seen in Fig. 9 have been approximated by one or several delta functions by Blunck and Leisegang (1950), by Talman (1979), and by Bak *et al.* (1987). The density effect is incorporated in this part; for the rest of the spectrum, the Rutherford cross section is used.

A closer approach to the present cross section was achieved by Bichsel (1970a), who used GOS for the K and L shells calculated with the screened hydrogenic matrix elements.

An interesting approach was used by Knop *et al.* (1961), by Bichsel (1974), and by Talman (1979), who separated $\sigma(E)$ into two parts: they used the Vavilov or Shulek functions for all electrons outside of the K shell, and convoluted it with the contribution for K-shell electrons calculated with the screened hydrogenic approximation.

Chechin and Ermilova (1976) used a harmonic-oscillator model to approximate the resonance collisions for argon. Lapique and Piuz (1980) discussed cluster counting and gave detailed information about the collision cross section for argon.

Allison and Cobb (1980) described the "photoabsorption ionization" (PAI) model: in their Eq. (28) they di-

vided the cross section into three parts similar to the division given in Eq. (3.8), but in Eq. (3.1) they used a variable value of Q_1, chosen to be equal to E. Equation (3.2) was unchanged. They approximated $\sigma_u(E)$ [Eq. (3.3)] with the Rutherford cross section, multiplied by a factor calculated from DOS:

$$\chi(E)=\int_0^E f(E',0)dE' , \tag{5.1}$$

which corresponds to $EA(E)$ of Eq. (3.3), but which is always less than 1 [Eq. (B3), Fig. 8]. Chechin *et al.* (1972) used essentially the same equation.

VI. METHODS FOR OBTAINING STRAGGLING FUNCTIONS

A variety of approximations (Sec. V) for the single collision spectrum have been used to calculate straggling functions with the following methods, given in order of appearance in the literature: (1) use of moments, (2) mixed-method calculations, (3) Laplace transformation calculations, (4) convolution calculations, (5) Monte Carlo calculations.

Bohr (1948), with statistical arguments, assumed that the straggling for relatively thick absorbers should be represented in a first approximation by a Gaussian function, with the most probable value Δ_p of the total energy-loss spectrum located at the mean energy loss $\langle\Delta\rangle=tM_1$ (Sec. IV) and with a standard deviation σ, given by $\sigma^2=tM_2$. Symon (1948) and Tschalär (1968a, 1968b) used the third moment M_3 to obtain the asymmetry of the straggling functions.

In mixed calculations, a straggling function obtained from a simple model of the collision spectrum (such as Bohr's Gaussian function) is convoluted with a function calculated from a residual term. Williams (1929), for example, divided the single collision spectrum into two parts: that for energy losses smaller than E_1 and that for energy losses above E_1. He used a Gaussian to approximate the straggling function for the collisions with $E<E_1$ and convoluted it with a function for the larger energy losses (which was obtained from convolutions of the Rutherford spectrum for $E\geq E_1$). Other mixed calculations were performed after the Landau function was published, and are described below.

In the third method, a transport equation describing the change in $f(\Delta)$ for a small increment in absorber thickness is derived. This equation then is solved with Laplace transforms. The method was first applied by Landau (1944), who used the Rutherford spectrum to obtain the "Landau straggling function" described in many of the references (see Appendix D). Its value of the most probable energy loss Δ_p and the full width at half maximum w are discussed in Appendix E.

Later, the Laplace-transform method was used with various modifications of the primary collision spectrum by Blunck and Leisegang (1950; Appendix F), Vavilov (1957), Shulek *et al.* (1966), Bichsel (1970a), and Talman (1979). It has been reviewed recently by Bichsel and Saxon (1975), Hall (1984), and others. The generic term "Shulek function" is introduced here to indicate the Landau, Vavilov, or Shulek *et al.* functions (Appendix D).

Further developments were achieved with mixed methods: Shulek functions were convoluted with the single collision spectrum for K-shell excitations when the average number of collisions with electrons in this shell was less than one [Knop *et al.* (1961), Bichsel (1974), and Talman (1979)].

A more complex mixed method was used by Bak *et al.* (1987). They calculated separate distribution functions for the resonance and the Coulomb-type collisions and used different approaches according to whether the number of collisions was smaller or larger than ten for each contribution. In the end, they obtained functions which for very thin absorbers showed a distinct peak for K-shell excitations, similar to the one given by Bichsel (1974) for Xe; the authors describe it as an "artificial feature of the model." Talman (1979) compared this approach (he described it as "treating the K shell discretely") with a calculation where he treated the K shell "continuously" and only found a peak for the "discrete" calculation. No peak appears in the convolution calculation for $t=10$ μm, Fig. 11, but in even thinner absorbers, individual plasmon peaks appear [Bichsel and Saxon (1975); Perez *et al.* (1977)]. The theoretical results of Bak *et al.* for the most probable energy loss differ by up to $\pm 4\%$ from those for the present theory for $t<300$ μm, and by 0.9–1.5 % for $t=1040$ μm. The results for w are up to 15% less for $t=32$ μm and up to 10% larger for $50<t/\mu\text{m}<200$. For $t=290$ μm, they differ by -1.2% to 1.5%; for $t=1040$ μm, by -2.2% to -3.3%.

A mixed-method equivalent to the Blunck-Leisegang approach was also used by Hancock *et al.* (1983) with a rather peculiar twist: the Landau parameter ξ as well as the most probable energy loss Δ_p (Appendixes D and E) were used as free parameters in the calculation of the Landau function, which then was convoluted with a Gaussian representing the resonance collision with a further free parameter, equivalent to δ_2 in the other theories (Appendixes G and H). The parameters were then adjusted until a good fit to the experimental data was obtained.

The interaction of the charged particles in the absorber is simulated most closely by a Monte Carlo calculation, the fifth method mentioned above. As for all other approaches, it is necessary to have a knowledge of the energy-loss spectrum $\sigma(E)$ for single collisions. In the calculation, the passage of each particle through the detector is followed from one collision to the next. The distance traveled between collisions as well as the energy loss E in the collision is determined with random numbers (Press *et al.*, 1986), and the individual energy losses are added up to the total energy loss Δ of the particle, Eq. (1.1). The calculation is repeated for N particles, and a function $f_1(\Delta)$ is thus generated. If different sets of random numbers are used for further calculations,

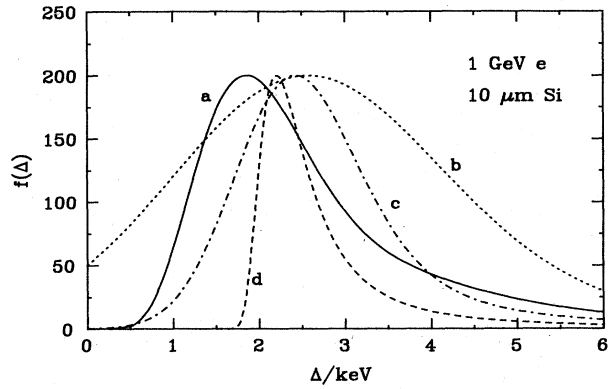

FIG. 11. Calculated energy-loss spectra $f(\Delta)$ for 1-GeV electrons passing through a silicon detector of thickness 10 μm. The ordinate is an arbitrary scale, and all spectra are normalized to the same peak height. The solid line *a* represents the spectrum calculated with the present theory. The other three lines—*b*, *c*, and *d*—represent Shulek functions (Appendix D) calculated with different values of δ_2 (Appendix G). For the dotted line *b*, the value $\delta_2=2130$ keV^2/cm was used. It is obtained from the primary collision spectrum used for line *a*. For the chained line *c*, $\delta_2=359$ keV^2/cm was used: the integral for M_2 of Eq. (4.1) extends to $E_u=1600$ eV only (Fig. 10). This value was chosen to give a Shulek function with the same width as that from the present theory. The Vavilov function (with $\delta_2=0$, $\kappa=3.6\times10^{-7}$) is shown as the dashed line *d*. It is equal to the Landau function. Parameters describing the various functions are

line	Δ_p	w	δ_2
a	1.857	1.758	
b	2.57	3.76	2130
c	2.42	1.76	358
d	2.21	0.717	0
e	2.51	2.8	1105

Function *e* is not shown; it is calculated with δ_2 according to the Shulek prescription (as suggested by Hancock *et al.*, 1983), using the Sternheimer parameters for silicon (Table X). It is 60% wider than function *a*. Clearly, the convolution of the Landau function with a Gaussian, i.e., the Blunck-Leisegang (1950) theory (Appendix F), will not give the correct shape of the straggling function: function *c* rises more slowly than function *a* below Δ_p and decreases faster above Δ_p. The reason for the small value of Δ_p of curve *a* compared to that for the Landau function is that *K*-shell electrons effectively do not contribute to the energy loss in function *a*, but they are included in function *d*. Indeed, the ratio of the Δ_p, $1.857/2.21=0.84$, is close to the ratio of electrons in $L+M$ shells to that of all shells: $12/14=0.86$. Note that Δ_p increases with increasing δ_2.

different functions $f_j(\Delta)$ will be obtained. This is the procedure of experimental measurements: in each repetition of the experiment, a different ionization function will be obtained. Monte Carlo calculations are time consuming (tens of hours on a VAX 780), and they can only give stochastic samples of the functions derived with analytic methods. Monte Carlo calculations for energy-loss distributions were proposed by Herring and Merzbacher (1957) and were performed by, among others, Ispirian *et al.* (1974), Cobb *et al.* (1976), Ermilova *et al.* (1977), and Brenner *et al.* (1981). A spectrum calculated with the Monte Carlo method was compared with those from other methods by Bichsel (1985b).

The randomness inherent in Monte Carlo calculations can be eliminated with the following analytic method, which implies that infinitely many particles pass through the absorber. An important assumption, though, is that successive collisions are statistically independent.[7] This assumption is confirmed by measurements with electron-energy-loss spectroscopy, and particularly by the fact that there are particles traversing the absorber without undergoing any collisions (Perez *et al.*, 1977). The number of collisions experienced by the particles then is described by the Poisson distribution

$$P(n)=\frac{m^n}{n!}e^{-m}\ , \tag{6.1}$$

where $P(n)$ gives the fraction of particles suffering n collisions, and m is the average number of collisions for all particles, calculated with the absorber thickness t and the total collision cross section M_0: $m=tM_0$. A fraction $P(0)=e^{-m}$ of the particles pass through the detector without a collision, the corresponding thickness is $t=-[\ln P(0)]/M_0$. For 45-GeV/c pions, $M_0=38\,400$ cm$^{-1}=3.84/\mu$m. Then, $P(0)=0.5$ for $t=0.18$ μm, and $P(0)=0.01$ for $t=1.2$ μm.

The probability density function for n collisions is given by the n-fold convolution of the single collision spectrum $\sigma(E)$:

$$\sigma(\Delta)^{*n}=\int_0^\Delta \sigma(E)\sigma^{*(n-1)}(\Delta-E)dE \tag{6.2}$$

with

$$\sigma(\Delta)^{*0}=\delta(\Delta)\ \text{ and }\ \sigma(\Delta)^{*1}=\sigma(\Delta)\ .$$

The complete straggling function then is

$$f(t,\Delta)=\sum_{n=0}^{\infty}\frac{m^n e^{-m}}{n!}\sigma(\Delta)^{*n}\ . \tag{6.3}$$

This approach to the calculation of $f(t,\Delta)$ is the "convolution method." It was considered by Herring and Merzbacher (1957) and later used by Kellerer (1968), who performed calculations with the Rutherford cross section. It was used with a more realistic collision spectrum for aluminum by Bichsel and Saxon (1975) and for argon by Allison and Cobb (1980).

Mathematically, the Monte Carlo-, the convolution-, and the Laplace-transform calculations are equivalent. Given an adequate primary collision spectrum, it is possible to obtain good energy-loss straggling functions with any of these three methods. The Laplace-transform

[7]In channeling, there is a correlation between successive angular deflections and energy losses.

method with a realistic collision spectrum was used by Bichsel (1970a). Straggling functions calculated with several methods are compared in Figs. 11–13.

In practice, it may be difficult to achieve satisfactory results with Laplace transforms because of numerical problems dealing with the sharp resonance peaks of the primary collision spectrum (Bichsel, 1970a). With the Monte Carlo method it is quite time consuming to achieve accurate results. There seem to be no serious problems with the convolution method. It is therefore used here.

VII. CONVOLUTION METHOD

The method in the form used for the calculations of Secs. VIII and X is reviewed here briefly. We assume that the straggling distribution $f(x,\Delta)$ has been determined for a certain absorber of thickness x. Then the function for an absorber of thickness $2x$ is calculated by the convolution of $f(x,\Delta)$ with itself:

$$f(2x,\Delta)=\int_0^{\Delta} f(x,\Delta-g)f(x,g)dg \ . \tag{7.1}$$

An initial distribution is calculated for an extremely thin absorber of thickness dx from

$$f(dx,\Delta)=\delta(\Delta)(1-M_0dx)+dx\ \sigma(\Delta) \ , \tag{7.2}$$

where $f(0,\Delta)=\delta(\Delta)$ and $M_0dx=n_0\approx 0.001$. This distribution now is convoluted with itself according to Eq. (7.1) until the desired thickness t is reached (Bichsel and Saxon, 1975).

The single collision spectrum $\sigma(E)$ described in Sec. III.D is calculated for the incident particles for energy losses E between 1.8 eV and the maximum energy loss E_u needed for a given absorber thickness. This is either the maximum energy loss E_M in a single collision, Eq. (3.6)—80 keV for 40-MeV protons, 500 MeV for 1-GeV electrons, 32 GeV for 45-GeV pions—or, according to Eq. (7.1), at most the highest total energy loss Δ_M for which $f(t,\Delta)$ is to be calculated (for the experiments described in Sec. X, Δ_M is less than 4 MeV). In the calculations it was found that a value $E_u=1.4$ MeV was sufficiently large to exclude truncation errors in the convolutions made here. Thus $\sigma(E)$ will extend to $E_u=1.4$ MeV or to E_M, whichever is smaller. A linear energy scale would not be practical for such a large range of energy losses. The numerical calculations were performed for energy-loss values equally spaced in $\ln E$. Most of the calculations were performed for a grid with $N_2=64$ values per factor of 2, i.e., 1250 values for the total spectrum. The accuracy of each convolution was checked by calculating the moments M_0 to M_3 of the resulting function. They were compared with the theoretical moments. Differences were always less than 0.3%. Further checks of the numerical accuracy of the results were made with numerical methods: for example, values of Δ_p and w calculated with $N_2=32$ rather than $N_2=64$ differed by less than 1% from the latter. Also, values calculated with $n_0\approx 0.0005$ in Eq. (7.1) differed by less than 0.01% from those with $n_0\approx 0.001$.

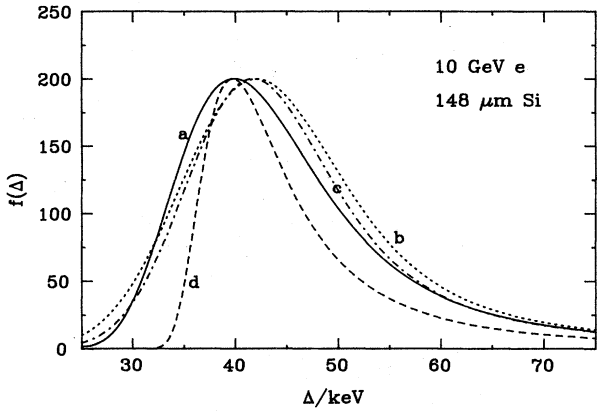

FIG. 12. Calculated energy-loss spectra $f(\Delta)$ for 10-GeV/c electrons passing through a silicon detector of thickness 148 μm. The solid line a represents the spectrum calculated with the present theory. The dotted line b is the spectrum calculated with the Shulek theory (Appendix D) and the value $\delta_2=2260$ keV^2/cm obtained from the primary collision spectrum used here (extending to $E_u=1.4$ MeV). The chained line c represents a calculation with a value $\delta_2=1615$ keV^2/cm, chosen to give a Shulek function with the same width as that from the present theory (Appendix G). The Vavilov function (with $\kappa=5.2\times10^{-7}$) is shown as the broken line d. Parameters describing the various functions are

line	Δ_p	w	δ_2
a	39.9	17.26	
b	42	19.16	2260
c	41.7	17.27	1615
d	39.7	10.60	0
e	41.4	15.56	1105

Function e is not shown; it is calculated with δ_2 according to the Shulek prescription, using the Sternheimer parameters for silicon (Appendix H). As in Fig. 11, the convolution of the Landau function with a Gaussian, i.e., the Blunck-Leisegang (1950) theory, will not give the correct shape of the straggling function.

The spectrum was transformed onto a linear scale of energy loss with a separate program. The most probable energy loss Δ_p was determined by a parabolic fit to the straggling function with the three values of the function nearest the maximum. The estimated uncertainty of Δ_p from this fit was less than 0.2%. The full width at half maximum w was determined by linear interpolation.

VIII. RESULTS OF ENERGY-LOSS CALCULATIONS

Many energy-loss spectra were calculated for the present study, especially for the cases differing substantially from other theories (e.g., very thin absorbers). The calculations were not very time consuming. For example, for 1-GeV electrons traversing a detector of thickness $t=2.5$ mm, 24 convolutions were needed. With $N_2=64$, the calculation took 7 min of CPU time on a

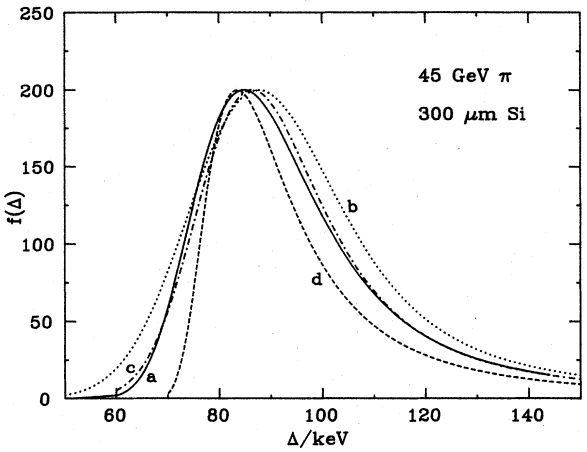

FIG. 13. Calculated energy-loss spectra $f(\Delta)$ for 45-GeV/c pions passing through a silicon detector of thickness 300 μm. The same functions are shown as in Fig. 12. The following parameters describe the functions:

line	Δ_p	w	δ_2
a	84.8	29.9	
b	87.7	35.8	3370
c	86.4	29.9	1794
d	83.5	21.5	0
e	85.8	27.0	1105

The last function is not shown; it corresponds to the experimental data presented by Hancock *et al.* (1983), but does not include the contribution from detector noise. The uncertainty of the measured Δ_p was ± 2.8 keV; of w, about ± 2.5 keV. The measured function thus does not disagree with the present theory, function *a*. Here, functions *a* and *c* show only a small difference in shape, but the Shulek function with δ_2 calculated according to Eq. (4.7), function *b*, is still much wider than function *a*.

VAX 780. With $N_2 = 32$, the calculation took 2 min.

Because energy-loss functions depend on both detector thickness and particle speed, it is not practical to give comprehensive tables or figures for them.[8] General trends can be seen from three examples of spectra, tables, and graphs of Δ_p and w for selected values of absorber thickness t and particle speed β, given next. Energy-loss spectra for 1-GeV electrons passing through a 10-μm silicon detector, calculated with several different approximations for the straggling function, are shown in Fig. 11. It is seen that none of the spectra calculated with the other theories is close to the spectrum obtained from the present theory. Spectra calculated for 10-GeV/c electrons passing through a silicon detector of thickness 148 μm are shown in Fig. 12. Again, none of the other theories is close to the present one. In particular, it should be noted that the functions calculated with the Shulek approximation rise less steeply and drop faster with increasing Δ than the present function. Finally, spectra calculated for 45-GeV/c pions traversing a detector of thickness 300 μm are shown in Fig. 13. Here, the Landau function and the Shulek function with $\delta_2 = 3370$ keV^2/cm (Appendixes G and H) differ strongly from present theory, while a Shulek function with $\delta_2 = 1794$ keV^2/cm differs only slightly, but again, it rises less steeply and drops faster.

Other examples of calculated spectra will be shown in the comparisons with the experiments in Sec. X. Clearly, the largest differences between the various theories occur for thin absorbers.

For some purposes it may be sufficient to consider only the values of Δ_p and w. It is a remarkable result of the calculations that Δ_p and w are independent of particle speed to within 0.1% for $\beta\gamma > 500$ (i.e., 250-MeV electrons, 70-GeV pions, and 500-GeV protons), i.e., there is no relativistic rise of Δ_p beyond $\beta\gamma = 500$ (see Appendix C). Values of Δ_p for $\beta\gamma > 500$ are given in Table V, those of w in Table VI. For $100 < \beta\gamma < 500$, Δ_p and w are within 1% of the values given in the tables. Functions useful for interpolation are also given. For thicknesses of 10, 80, and 1280 μm, Δ_p is given as a function of $\beta\gamma$ in Fig. 14. Also given is $w(\beta\gamma)$ for $t = 320$ μm. For mesons and protons, and the thicknesses shown in the tables, Δ_p and w differ by less than 0.1% from the values for electrons. For much thicker absorbers, differences will appear because of multiple scattering, nuclear reactions, etc.

A more detailed representation of w as a function of absorber thickness for $\beta\gamma > 500$ is given in Fig. 15, which corresponds to Fig. 4 in Bak *et al.* (1987). The ratio w/w_L is shown as the solid line ($w_L = 4\xi$). This function agrees within a few percent with that of Bak *et al.* for $t > 70$ μm, but it is almost twice as large at 20 μm. Maybe of even greater interest is the second ratio shown: that of w to w_S, the width of the Shulek function (dashed line). The small values of w relative to w_S for $t < 15$ μm can be understood qualitatively: for very thin absorbers, the probability of interactions with K-shell electrons is very small. Effectively, only 12 electrons contribute to the energy-loss processes. This also causes a large reduction in δ_2, from that for all three shells, $\delta_2 = 2130$ keV^2/cm, to that for only the L and M shell, approxi-

[8] On a limited basis, calculated spectra can be obtained from the author. A graph of the measured spectrum should be sent to him. It will be returned with the calculated function. Requirements: On the graph, w should be greater than 6 cm; the height of the spectrum should be 10 cm or more. The abscissa (indicating pulse height or ionization) must be linear. The experimental arrangement (beam line, detector position, collimators) must be described, and absorber thickness, particle type, and energy spectrum (or spectrum of momentum or $\beta\gamma$), and noise contribution (w_n or σ_n) must be given. If there are contributions from sources other than the particles under consideration, they either must be subtracted or the spectrum must be given for pulse heights at least $\pm 2w$ from Δ_p. The effects discussed in Sec. IX must be described (see Bak *et al.*, 1987, for a good example). It would be useful if the moments M_0 to M_3 of the measured spectrum were provided. Alternatively, a listing of the data in ASCII code on a 5.25-in. floppy disk readable by an IBM PC-AT can be sent.

TABLE V. Values of the most probable energy loss Δ_p of the energy-loss straggling functions $f(\Delta)$ as a function of thickness t of a silicon absorber for all particles with charge $\pm 1e$ and $\beta\gamma > 500$ (250-MeV electrons, 70-GeV pions, and 500-GeV protons). For $\beta\gamma > 100$, Δ_p differs by no more than 1% from the values given in column 2. The absolute uncertainty of Δ_p is estimated to be less than $\pm 1\%$ (one standard deviation), the relative error about 0.1%. The following functions (Bichsel, 1987) approximate Δ_p (eV) to within 1.2% for $\beta\gamma > 100$ (t in μm): $13 < t < 110$, $\Delta_p = t(100.6 + 35.35 \ln t)$; for $110 < t < 3000$, $\Delta_p = t(190 + 16.3 \ln t)$. The ratio r_p of Δ_p to the values ${}_L\Delta_p$ calculated with the Landau theory (Appendix E), as well as the ratio Δ_p/t (eV/μm), is given. For comparison, the mean energy loss $\langle\Delta\rangle_\pi$ for 100-GeV pions ($\beta\gamma = 717$, $E_M = 84.2$ GeV, $dT/dt = 0.555$ keV/μm) calculated with Eq. (4.2) is given as well as that for 1-GeV electrons ($dT/dt = 0.4888$ keV/μm, from ICRU, 1984).

t (μm)	Δ_p (keV)	r_P	Δ_p/t	$\langle\Delta\rangle_\pi$	$\langle\Delta\rangle_e$
10	1.857	0.844	186	5.55	4.9
20	4.120	0.886	206	11.1	9.8
40	9.282	0.948	232	22.2	19.6
80	20.39	0.991	255	44.4	39.1
160	43.38	1.006	272	88.7	78.2
320	90.96	1.008	285	177	156
640	189.4	1.006	296	355	313
1280	393.2	1.002	307	710	626
2560	815.5	0.999	319	1420	1251

mately $\delta_2 = 800$ keV^2/cm (Bichsel, 1985a; see also Fig. 10 and Appendix G). The Landau theory begins to approximate the correct values of w only for $t \gg 2$ mm, the Shulek theory for $t > 800$ μm.

Thus it appears that straggling functions must be calculated with the present theory for all experimental situations where close agreement between theory and experiment is to be found. In particular, the Landau value of Δ_p is larger than the value calculated with the present theory for $t < 100$ μm (see Table V), and the Landau width $w_L = 4\xi$ is much smaller than that given by the present theory (Fig. 15). On the other hand, the Shulek *et al.* (1967) theory gives values w_S much larger than the present theory.

Since the present theory furnishes absolute values of Δ_p, it must be considered the preferred method to be used for the energy calibration of silicon detectors (see Sec. X.C). It is necessary, though, that the thickness of the sensitive region of the detector be known accurately, and that the noise contribution and other effects discussed in Sec. IX be determined reliably.

The following sources of errors of the calculated straggling functions must be considered: (a) errors in the primary collision spectrum and (b) errors in the convolution calculation.

An estimate of the influence of errors in the primary collision spectrum can be obtained from straggling functions calculated with different collision spectra. This was

TABLE VI. Values of the full width at half maximum, w of the straggling function $f(\Delta)$ as a function of thickness t of a silicon absorber for all particles with charge $\pm 1e$ and $\beta\gamma > 500$. The absolute uncertainty of w is estimated to be $\pm 1\%$, the relative error about 0.1%. For $\beta\gamma > 100$, w is within 1% of the values in column 2. The ratio r_L of w to the values calculated with the Landau theory ($w_L = 4\xi$) is given, as well as the ratio $r_S = w/w_S$, where w_S is the width of the Shulek function (Appendix D), with $\delta_2 = 2130$ keV^2/cm. The ratio of Δ_p (from Table V) and w is also shown. No simple relations between the thickness and any of the three functions can be discerned in the table; but the following approximation functions given w (in eV) with an error of less than 2% (t in μm): $5.7 < t < 11$, $w = t(298.3 - 53.53 \ln t)$; $11 < t < 30$, $w = t(174.7 - 2.72 \ln t)$; $30 < t < 260$, $w = t(259.6 - 28.41 \ln t)$; $260 < t < 2560$, $w = 71.3t(1 + 39.4/t^{0.8})$. Since the ratio Δ_p/w depends on absorber thickness, it can be used to infer the detector thickness from it. Great care must be taken, though, to determine all the corrections discussed in Sec. IX (see Table IX).

t (μm)	w (keV)	r_L	r_S	Δ_p/w
10	1.758	2.465	0.468	1.05
20	3.338	2.341	0.605	1.234
40	6.291	2.206	0.764	1.475
80	10.818	1.897	0.860	1.885
160	18.32	1.606	0.923	2.369
320	31.54	1.382	0.965	2.884
640	55.98	1.227	0.989	3.383
1280	103.01	1.128	1.000	3.817
2560	195.8	1.073	1.005	4.165

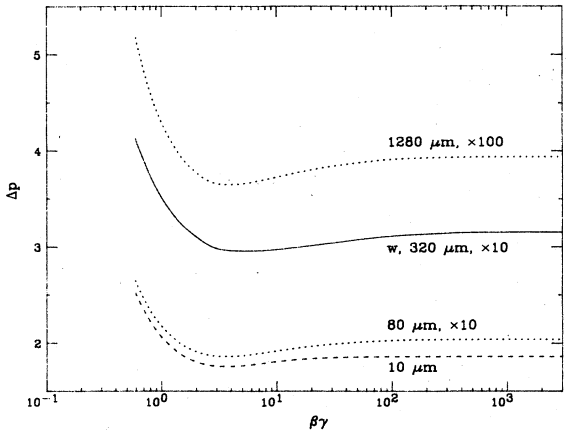

FIG. 14. Most probable energy loss Δ_p (keV) for $t=10$, 80, 320, and 1280 μm as a function of $\beta\gamma$. Also given is w for $t=320$ μm. The values must be multiplied by the factors shown (see Tables V and VI). The values are expected to be constant for large values of $\beta\gamma$ because they are determined only by energy losses less than about $2\Delta_p$. For these energy losses, $\sigma(E)$ is almost independent of particle energy for $\beta\approx 1$ (see Appendix C).

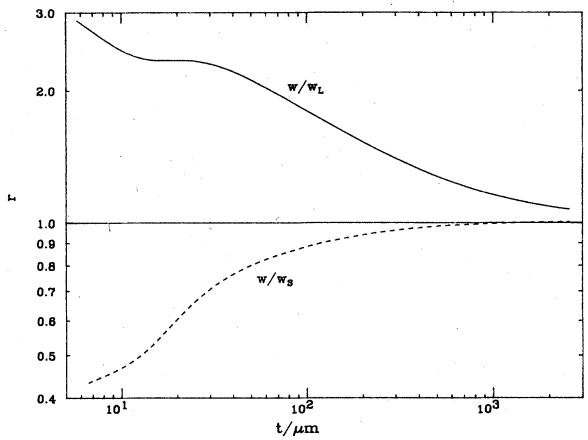

FIG. 15. Ratio r of the full width at half maximum w of the present straggling function to the Landau width $w_L=4\xi$ as a function of thickness t of a silicon absorber for particles with $\beta\gamma>500$. The leveling in the ratio for $16<t<25$ μm is due to the increase from very small values to 1 and more in the probability of collisions with K-shell electrons. Also given is the ratio r of w to the width w_S of the Shulek function (Appendix D), calculated with $\delta_2=2130$ keV^2/cm (the value for 1-GeV electrons, using the upper limit $E_u=1.4$ MeV in the integral; see Sec. IV.D). For small thicknesses, w is much less than w_S—again indicating that the K-shell electrons do not contribute significantly to the energy losses. For heavy particles, δ_2 would be larger, and therefore r would be smaller.

done with three of them (Table VII): (a) the one used here, (b) the one used in earlier calculations (Bichsel, 1985a), (c) the PAI model described by Allison and Cobb (1980; see also Sec. V) and applied here to silicon.

The major uncertainties of spectrum (a) were described in Sec. III.D. For (b), a major error was that the optical constants were determined separately for each shell. In particular, the Kramers-Kronig relation used to calculate ε_1 from ε_2 was applied for each shell. Furthermore, the calculations of the generalized oscillator strength were made only for energy losses of less than 220 Ry. For PAI, the values of the complex dielectric constant $\varepsilon(E)$ derived in Sec. II.E were used, but GOS was calculated with the approximation of Eq. (5.1). A comparison between the spectrum $\sigma(E)$ used here and that which was calculated with the PAI approximation shows differences of 5–10 % for most of the spectrum, but differences of up to 40% occur just beyond the plasmon peak at $E=16.8$ eV. The total collision cross sections M_0 calculated with the two spectra for 1-GeV electrons were 38 388 and 40 942 collisions/cm, i.e., the PAI value is 6.7% larger than the one used here. The stopping power is only 0.8% larger, though. Energy-loss spectra were calculated with these three $\sigma(E)$ for the following cases: 45-GeV/c pions in 300 μm of silicon, 42.4-MeV protons in 196 μm, and 1-GeV electrons in 10 μm. The results are shown in Table VII. The maximum difference seen in the table for Δ_p amounts to 4% for the very thin absorber, that for w to 1.8% for the thick absorber. Errors in the convolution calculations were discussed at the end of Sec. VII.

IX. IONIZATION IN A SILICON DETECTOR

Usually, the energy lost, Δ [Eq. (1.1)], by a charged particle traversing an absorber is deposited in it. If a large energy loss occurs, it is possible that a delta ray will have enough energy to escape from the detector. Then the energy deposited in the absorber, Δ', is less than the energy lost, Δ (Laulainen and Bichsel, 1972; Hall, 1984). The Monte Carlo calculations by Bichsel (1985b) for 100-MeV protons, traversing the equivalent of 1 μm of

TABLE VII. Values of Δ_p and w, calculated with three different single collision spectra $\sigma(E)$ for 45-GeV/c pions in 300 μm of silicon, 42.4-MeV protons in 196 μm, and 1-GeV electrons in 10 μm (see end of Sec. VIII).

	45 GeV/c π		42.4 MeV p		1 GeV e	
	Δ_p (keV)	w (keV)	Δ_p (keV)	w (keV)	Δ_p (keV)	w (keV)
(a)	85.58	29.85	484	139.4	1.858	1.758
(b)	87.66	29.59				
(c)	87.15	29.33	493	138.4	1.931	1.756

silicon, showed changes in the spectrum no greater than the stochastic variations ($\pm 1.5\%$ to $\pm 5\%$) for $0.2 < (\Delta/\Delta_p) < 2$. Large changes were found only for $\Delta > 5\Delta_p$. In Sec. X experimental spectra for $\Delta < 3\Delta_p$ were compared with the theory: we can expect that the effects of δ-ray escape will be very small.

The energy losses of the charged particle cause ionization in the silicon, both in the primary collision and by the subsequent energy loss of the secondary electrons. A detailed discussion of the sequence of events in ionization processes is given, for example, by Herring and Merzbacher (1957). Usually, the energy loss in primary collisions (see Figs. 9 and 10) is larger than the average energy W needed to produce an electron-hole pair (approximately 3.7 eV). Thus, for each collision of the incident particle, several electron-hole pairs will be produced.

No complete theory of the relation between the energy deposited by a charged particle in silicon, Δ', and the consequent ionization J (expressed as a number of electron-hole pairs) is available (see Antoncik *et al.*, 1970, though). An empirical approach is used here: it is assumed that there is a proportionality factor W (ICRU, 1979;[9] L'Hoir, 1984; Lennard *et al.*, 1986) relating Δ' and J: $J = \Delta'/W$. It is known that (a) $W \approx 3.7$ eV at 300 K; (b) W does depend on particle type; (c) for heavy, slow ions, W depends on the ion speed; (d) the dependence on ion velocity for particles with charge $\pm 1e$ seems to be small; (e) for heavy ions, with energies of 100–700 MeV/u, Schimmerling *et al.* (1983) showed an increase in W for gases of 10%, (f) W is temperature dependent; and (g) W depends on the concentration of crystal imperfections (Geretschläger, 1987).

For electrons losing their full energy in the detector, the energy dependence of the integrated W, in a first approximation for $E \gg b$, is given by $W(E) \approx W_0/(1-b/E)$, where $b = 1.08$ eV is the band gap for silicon (ICRU, 1979; Lægsgaard, 1982: For 0.56-keV electrons, W increases no more than 1% over W for 6-keV electrons). Thus changes in the δ-ray spectrum with particle speed would cause changes in W. Preliminary calculations with a model proposed by Bichsel and Inokuti (1976), using $\sigma(E,v)$, showed that changes in W of the order of 0.3% due to this effect might be expected for the speeds considered here.

Effects that must be considered in the comparison of theoretical and experimental spectra are described next, with an outline of the action needed to include the effect. Usually, additional data about the experiment must be provided.

(a) Detector and amplifier noise: a Gaussian of width σ_n given by the experimenters is convoluted with the ionization spectrum.

(b) Statistical variations of the number of particles counted in each ionization bin of the spectrum: check whether deviations from the theoretical spectrum are distributed according to a Poisson distribution.

(c) Statistical fluctuations in the number of electron-hole pairs produced (they are smaller than 1% for the experiments described in Sec. X).

(d) A correction for saturation (incomplete collection of charges) must be made in the experiment; it is usually disguised by the "energy calibration" (e.g., Aitken *et al.*, 1969).

(e) Errors in determination of the depletion layer or of the detector thickness (Croitoru *et al.*, 1985): calculated values of Δ_p and w will both be different from the measured values. If the energy calibration is correct, calculations with different values of t can be made until agreement is achieved, and t thus can be determined (e.g., Bichsel, 1985a; see also Table VIII).

(f) Inhomogeneity of detector thickness: this would cause an experimental distribution wider than the calculated one. Measurements of the inhomogeneity must be made, then spectra calculated for the various thicknesses are added together. The thickness inhomogeneity can be measured if a beam with a very small cross-sectional area is used (Bichsel *et al.*, 1957; Møller, 1986).

(g) Nonlinearity of amplifier–multichannel-analyzer system: the system must be calibrated with a precision pulser at the same input connection as that where the silicon detector is connected. It is especially important to determine the intercept of the channel number versus pulse-height curve (Hanke and Bichsel, 1970).

(h) Energy spread in particle beam or admixture of other particles in the beam observed in the detector [e.g., electrons and muons in a pion beam (Bak *et al.*, 1987)]: theoretical ionization spectra must be calculated for each particle and energy and then added to give the spectrum to be compared with experiment.

(i) Radiation from other sources (e.g., bremsstrahlung, δ rays from surface layers, collimators, and enclosures): it would be necessary to establish the source spectrum of such radiation, calculate the ionization spectrum, and combine it with the spectrum of primary interest.

(j) Internal bremsstrahlung of the detector: see Appendix I.

(k) Systematic errors of the theory: back to the drawing board.

For the comparison of theory and experiment, it would also be useful if the total number N of particles passing through the detector were given, as well as the number of channels used in the pulse-height analyzer in which N was counted. Furthermore, values of the first, second, and third moment over the measured spectrum might be compared with theoretical values.

X. COMPARISON WITH EXPERIMENTS

A. Procedure

In order to obtain a straggling function for comparison with a measurement, it will be necessary to perform the

[9]As used in this paper, W is the "differential value w" on p. 1 of the reference.

TABLE VIII. Comparison of theoretical and experimental straggling functions for the data given by Bak *et al.* (1987). Protons: $\beta\gamma = 2.1$ and 8.5; pions; 14 and 57; electrons: 3914 and 15 700. The sign of the particle is given in front of w_x and ${}_x\Delta_p$. Detector thickness t in μm; particle speed $\beta\gamma$; noise σ_n in keV; theoretical and experimental widths of ionization curve, w_i and w_x, in keV; relative difference [Eq. (10.2)] between the two, r_w, in %; theoretical and experimental values of Δ_p in keV; and relative difference r_p in %. For each thickness, the average values of the r, as well as the σ_x, are given. In the last line, average values of the r and σ are given for all data in the table.

t	$\beta\gamma$	σ_n	w_i	w_x	r_w	${}_i\Delta_p$	${}_x\Delta_p$	r_p
32	2.1	0.78	5.198	5.36	3.0	7.397	7.128	−3.6
32	14	0.78	5.172	5.26	1.7	7.092	6.911	−2.6
32	3914	0.78	5.611	5.49	−2.1	7.36	7.137	−3
		$\langle r_w \rangle = 0.9 \pm 2.6$				$\langle r_p \rangle = -3.1 \pm 0.5$		
51	2.1	0.73	7.318	7.446	1.7	12.325	12.64	2.6
51	14	0.73	7.201	7.252	0.7	11.840	11.79	−0.4
51	3914	0.73	7.861	7.74	−1.5	12.397	12.24	−1.3
		$\langle r_w \rangle = 0.3 \pm 1.6$				$\langle r_p \rangle = 0.3 \pm 2$		
100	2.1	2.0	13.468	13.43	−0.3	26.356	26.76	1.5
100	14	2.0	12.929	13.29	2.8	25.283	25.96	2.7
100	3914	2.0	13.836	13.97	1	26.544	26.86	1.2
		$\langle r_w \rangle = 1.2 \pm 1.6$				$\langle r_p \rangle = 1.8 \pm 0.8$		
174	2.1	3.5	21.80	22.5	3.2	48.05	49.28	2.6
174	8.5	3.5	20.28	19.79	−2.4	44.985	45.18	0.4
174	14	3.5	20.50	21.08	2.8	45.92	47.3	3
174	57	3.5	21.17	20.58	−2.8	47.57	47.42	−0.3
174	3914	3.5	21.64	21.63	0	48.225	48.96	1.5
174	15 700	3.5	21.64	20.61	−4.8	48.225	47.77	−0.9
		$\langle r_w \rangle = -0.7 \pm 3.2$				$\langle r_p \rangle 1.0 \pm 1.6$		
290	2.1	3.2	31.63	31.01	−2.0	82.46	82.07	−0.5
			31.63	−29.18	[−7.7]	82.46	−81.63	−1.0
290	8.5	3.2	28.62	28.53	−0.3	76.91	75.89	−1.3
290							−77.99	1.4
290	14	3.2	28.87	28.91	0.1	78.49	77.54	−1.2
290		3.2	28.87	−28.81	−0.2		−77.73	−1.0
290	57	3.2	29.73	29.24	−1.6	81.30	79.43	−2.3
290		3.2	29.73	−29.24	−1.6		−79.73	−1.9
290	3914	3.2	30.38	30.21	−0.5	82.47	80.97	−1.8
290		3.2	30.38	−30.21	−0.5		−81.1	−1.7
290	15 700	3.2	30.38	29.28	−3.6		80.36	−2.6
				−30.32	−0.2		−81.14	−1.6
		$\langle r_w \rangle = -1.0 \pm 1.2$				$\langle r_p \rangle = -1.5 \pm 0.6$		
1040	2.1	3.9	97.46	93.13	−4.4	321.6	326.2	1.4
						321.6	−321.2	−0.1
1040	8.5	3.9	84.24	85.43	1.4	296.9	302.8	2.0
			84.24	−87.68	4.1		−311.1	4.8
1040	14	3.9	84.18	84.51	0.4	302.3	308.2	2.0
1040		3.9	84.18	−83.95	−0.3	302.3	−308.3	2.0
1040	57	3.9	85.17	84.12	−1.2	312.3	315.9	1.2
			85.17	−86.71	1.8	312.3	−314.1	0.6
1040	3914	3.9	86.22	86.5	0.3	316.7	320.4	1.2
1040		3.9	86.22	−86.31	0.1	316.7	−320.4	1.2
1040	15 700	3.9	86.22	83.54	−3.1	316.7	321.9	1.6
			86.22	−87.8	1.8	316.7	−316.7	0
		$\langle r_w \rangle = 0.1 \pm 2.4$				$\langle r_p \rangle = 1.5 \pm 1.3$		
All points (except −7.7%)				$\langle r_w \rangle = -0.2 \pm 2.2$			$\langle r_p \rangle = 0.1 \pm 1.9$	

convolution calculation for the energy losses outlined in Sec. VII followed by the calculation of the modifications caused by the experimental arrangement (Sec. IX).

In all experiments described here, the authors converted ionization in the detector into energy deposited in it by providing an energy calibration. They assumed that W was a constant for all particles of all speeds and independent of detector thickness. A systematic difference between measured and calculated spectra may indicate a speed or particle dependence of W. Among the effects (a)–(j) of Sec. IX, only the noise contribution [item (a)] is taken into account explicitly. Other effects will be considered for each experiment.

The location of the most probable value of the theoretical ionization spectrum will be designated by ${}_i\Delta_p$; the width by w_i. While these values should be expressed as "numbers of electron-hole pairs, J," they are written here in terms of energy deposition $W(T)J$. The value w_t calculated with (Maccabee *et al.*, 1968)

$$w_t^2 = w^2 + w_n^2 \tag{10.1}$$

will give values several percent different from w_i (Table IX). Similarly, there is no simple relation giving the change of the value of the most probable energy loss Δ_p with the amount of noise: Δ_p will increase by a few percent, and the convolution of the energy deposition spectrum with the noise spectrum cannot be avoided.

The presence of other effects (e.g., stray radiations or the escape of delta rays) will be seen if the experimental and theoretical functions are compared in detail (Sec. X.D).

Only experimental data with $\kappa < 0.6$ [Eq. (D7)] were compared with the present theory. They were found in ten recent papers.[10] The conversion of ionization spectra $\varphi(J)$ into energy deposition spectra $\varphi(\Delta)$ by the authors was accepted as given, and the differences between theoretical energy-loss and energy deposition spectra were neglected. The authors frequently did not provide complete information about the measured data. For example, Hancock *et al.* (1983, 1984) did not give measured values of Δ_p and w, and they only gave an average value of the noise contribution. Various problems in other experiments will be mentioned below. For the data where no value of the noise contribution σ_n was given, I have assumed plausible values, shown in Table IX.

A simple evaluation of theory and experiment can be obtained from a comparison of the measured, w_x, and the calculated, w_i, widths of the ionization spectrum, and of the values of the most probable energy losses, ${}_x\Delta_p$ and ${}_i\Delta_p$. These values are given in Tables VIII and IX. The comparison is made by calculating the relative differences r,

$$r_w = (w_x/w_t) - 1, \quad r_p = ({}_x\Delta_p/{}_i\Delta_p) - 1 , \tag{10.2}$$

and their standard deviations σ_x, given by

$$\sigma_x^2 = \sum_i (r_i - \langle r \rangle)^2/(n-1)$$

given in Table VIII and Figs. 16 and 17. Data were found for electrons, pions, protons, and α particles, with detectors ranging from 32 to 3000 μm. For these data, the calculated values of w and Δ_p for a given value of $\beta\gamma$ change by less than 1 part in 10^3 for particles with different masses and positive or negative charges. Thus the most suitable variable to indicate the particle energy is $\beta\gamma$.

The most extensive data set was given by Bak *et al.* (1987), discussed in the next section. In a separate section, W values are derived from this experiment. Other data are discussed in Sec. X.D.

B. CERN-1986 data

This set of experimental data given by Bak *et al.* (1987) is well suited for a comparison with the present theory. Data were taken for six silicon detector thicknesses from 32 to 1040 μm for values of $\beta\gamma$ between 2 and 15 700. Care was taken to eliminate most contamination by radiations other than the desired one. The noise contribution from detectors and amplifiers was measured carefully, the detectors were calibrated frequently, and a variety of the effects mentioned in Sec. IX were studied (Møller, 1986). The data are compared with the theory in Table VIII. The following observations may be made about these data.

(1) The average values of the relative differences for all data points (except -7.7%) are $\langle r_w \rangle = (-0.2 \pm 2.2)\%$ and $\langle r_p \rangle = (0 \pm 1.9)\%$: the agreement between theory and experiment is excellent, and the standard deviation σ_x of the experimental values is about $\pm 2\%$. The exclusion of the data for $t = 32$ μm would not change $\langle r_w \rangle$, but $\langle r_p \rangle$ would change to $(0.3 \pm 1.8)\%$.

(2) For $t = 50.9$, 100.3, and 290 μm, both $\langle r_w \rangle$ and $\langle r_p \rangle$ differ by similar amounts from zero, suggesting a systematic error in the detector thickness. Values of $t = 51.05$, 101.8, and 286.6 μm would give zero average deviation. The values for $t = 174$ and 1040 μm show larger variations than the others, and no need for a change in t can be discerned.

For $t = 32$ μm, the differences r_p are rather large. From the experimental side, it is possible that edge effects were larger than estimated. Then ${}_x\Delta_p$ would tend to be smaller than calculated from the nominal t, and w_x would be larger. An indication of this possibility is seen in Fig. 18, where the slope of the experimental straggling function between 3 and 7 keV is less than for the calculated function. Since this detector was cooled to 77 K, it is possible that the temperature dependence of W may have influenced the measured values of the energy loss. The possibility of errors in the theory cannot be excluded.

[10] Several earlier papers mentioned by Maccabee *et al.* (1968) and Aitken *et al.* (1969) agreed with the present theory within experimental limitations.

(3) The distribution of values of r_w around the mean value is consonant with a Gaussian distribution: 68% of the values are less than σ_x, 27% lie between σ_x and $2\sigma_x$, and two values exceed $2\sigma_x$ (one of these was not included in the mean). For r_p, the situation is similar.

Experimental and calculated spectra are compared in Figs. 18–21. An adjustment of the energy scales of the experimental data was made (i.e., the energy-loss scale was shifted to give the value of ${}_x\Delta_p$ equal to ${}_i\Delta_p$). For most data, the theoretical function goes to zero with decreasing Δ faster than the experimental one. Bak *et al.* (1987) ascribe this difference to "edge effects." No discernable change in the shape of the spectrum due to delta-ray escape is seen (see Laulainen and Bichsel, 1972, though). The agreement between theory and experiment is very good within the stochastic variation of the latter, while the Shulek functions differ much from the experiments.

C. Energy per electron-hole pair, *W*, in silicon for relativistic particles

Since the present theory provides absolute values Δ of the energy losses, while the experiments provide the ionization J corresponding to Δ', values of W can be derived from the comparison of Δ' and J from the experimental data given by Bak *et al.* (1987).

Both w and Δ_p of Table VIII can be used for this purpose. The theoretical quantities are the energy losses (in keV). Since very little energy is exported from the detector by δ rays for the experiments described here, Δ' and w' differ negligibly from Δ and w. While the experimental quantities are listed as energy losses, they actually are values of the ionization J and were converted into energy losses by the calibration procedure, which was performed with x and γ rays from ^{133}Ba using an implicit value of the integrated W for electrons (ICRU, 1979).

If $W(T)$ is almost constant for electrons (Lægsgaard, 1982),[11] the integrated value used for the calibration radiation is equal to the differential value needed for the transmitted particles. I shall postulate this and use the value $W=3.68\pm0.02$ eV at 300 K given in ICRU (1979). If now the calculated energy losses agree with the measured ones, as indeed they do, it follows that W for high-energy particles is the same as that for the calibration electrons. Furthermore, since all measured values agree on the average with the theoretical values within $\pm2\%$, we can conclude that W for all the particles $(e^{\pm},\pi^{\pm},p^{\pm})$ and all the speeds given in Table VIII is equal to 3.68 ± 0.07 eV.

Similarly, there is no evidence for any different value from the data in Table IX, except possibly for $\beta\gamma>30\,000$ in the data of Ogle *et al.* (1978). Further measurements at these speeds would be desirable.

[11]For 0.56-keV electrons, W increases no more than 1% over W for 6-keV electrons.

It is conceivable that systematic errors in the dependence on speed or particle type of the theory of energy loss could cancel systematic dependencies of W.

D. Comments about other experimental data

Theoretical and experimental values for the following references are given in Table IX.

Kolata *et al.* (1968): The values of ${}_x\Delta_p$ and w_x were read from the figures, and no error estimates were made. Only the two highest energies were considered, because for the lower energies the assumption of a constant speed of the protons in the absorber was less and less valid. The influence of the reduction in energy in the absorber can be assessed from calculations for two different energies, viz., 38.0 and 37.5 MeV, i.e., the incident energy and the most probable energy of protons leaving the foil. The values of Δ_p differ by 6 keV (1% of Δ_p), but w differs by only 0.03 keV.

Maccabee *et al.* (1968): Most of the experimental functions shown by the authors agreed quite closely with the Vavilov (1957) theory. The exception was 730-MeV protons in a detector with $t=464$ μm ($\kappa=0.0055$), $w_x=59.6$ keV. The authors used Eq. (10.1) with $w_n=35$ keV (i.e., $\sigma_n=15$ keV) to calculate an "actual width of $w=48.2$ keV," which then agreed with the "theoretical width of 48.4 keV" from the Vavilov theory. Since, from the present theory, $w=53.8$ keV, calculations were made with $\sigma_n=10$ keV ($w_n=24$ keV) as well as $\sigma_n=15$ keV (Table IX). Clearly, the smaller value agrees more closely with the experiment and would also be in line with "resolutions widths ($w_n=20-30$ keV)" given by the authors. If indeed the detector resolution was 35 keV, the value w_i calculated with the present theory would be 68 keV, or 14% larger than the measured value (Table IX). Thus a reexamination of the experimental resolution would be desirable.

Aitken *et al.* (1969): I assumed that the quantity E_{peak} given in the figures was ${}_x\Delta_p$, and obtained values of w_x by measuring them in Figs. 2, 3, and 5 in the paper, assuming that the channel number was proportional to the observed ionization and that channel zero corresponded to zero ionization. No values of σ_n were given, and plausible values were assumed (Table IX). For 458-MeV electrons in a 2-mm detector, the effect of internal bremsstrahlung should be discernable. It will be small compared to the resonance contribution (given by $w/w_L=1.094$), and cannot be determined in this experiment because the noise contribution is not known (see Appendix I).

Hancock *et al.* (1983, 1984): The quantity E_{mp} given by the authors in their Table II (and Table I) was considered to be ${}_x\Delta_p$. In order to obtain values of the experimental full width at half maximum w_x, I calculated the functions shown in the authors' Eq. (3), where the Landau function is convoluted with a Gaussian of standard deviation $\sigma^2=(\delta_2+\sigma_n^2)$; δ_2 is a free parameter given in

TABLE IX. Comparison of theoretical and experimental straggling functions for silicon detectors. Only data for which κ was less than 0.6 were considered. First, a symbol for the particle is given. The detector thickness t is given in μm, the particle energy T in MeV, and the standard deviation σ_n of the noise function in keV (the full width at half maximum of the Gaussian used for this purpose is $w_n = 2.355\sigma_n$). For some experiments, σ_n was given by the authors; for others, I chose a plausible value. In some cases, two values of σ_n were used, and for the second value, only σ_n, w_i, and ${}_i\Delta_p$ are given. The importance of an exact determination of σ_n can be assessed from these data. Three values are given for the width of the straggling functions: the width w (in keV) of the energy-loss function, the width w_i (keV) of the calculated ionization function, and the width w_x (keV) of the experimentally measured function. The comparison of w and w_i shows for which circumstances the noise contribution is important. The calculated value of the most probable energy deposition is ${}_i\Delta_p$ (keV); the measured value is ${}_x\Delta_p$. We note that ${}_x\Delta_p$ is in fact determined from the number of ion pairs produced (including the noise contribution), multiplied by the average energy W needed to produce an electron-hole pair. The noise contribution increases Δ_p by at most a few percent; therefore Δ_p for the energy-loss functions is not given. Notes and comments about the experiments are given in Sec. X.D. If errors for w_x or ${}_xD_p$ were given by the authors, they are listed on the same line as the name, in the appropriate column. The average differences between theory and experiment, $\langle r_w \rangle$ and $\langle r_p \rangle$, are given below the data. If more than three values are available, the average deviation is also given. Systematic errors might be hidden behind these averages.

	t	T	$\beta\gamma$	σ_n	w	w_i	w_x	${}_i\Delta_p$	${}_x\Delta_p$
Kolata *et al.* (1968)									
p	196	38	0.29	8	140.2	141.5	141	537	534
p	196	42.4	0.30	8	138.3	139.4	139	484	485
		average differences				$\langle r_w \rangle = -0.3$			$\langle r_p \rangle = 0.2$
Maccabee *et al.* (1968)							$\approx \pm 3\%$		$\pm 2\%$
α	245	895	0.73	9	197.0	198.4	200	671	678
α	884	910	0.74	10	598.3	598.8	619	2587	2610
p	464	730	1.47	10	53.8	60.6	59.6	161	157
				15		68		163	
p	1 772	730	1.47	10	188.4	190.4	184	664	659
		average differences				$\langle r_w \rangle = 0.3 \pm 3$			$\langle r_p \rangle = 0.3 \pm 2$
Aitken *et al.* (1969)									
p	2 160	315	0.89	20	333.6	338.0	360	1246	1329
π	2 160	65.3	1.07	20	281.2	286.5	296	1031	1061
e	2 160	458	897	20	166.8	176.1	176	686	687
				10		169.2		683	
		average differences				$\langle r_w \rangle = 3$			$\langle r_p \rangle = -3$
Hancock *et al.* (1983, 1984)							$\pm 8\%$		$\pm 3\%$
p	300	220	0.72	5	66.5	67.9	71	192	210
p	300	254	0.78	4	60.6	61.6	68	174	196
p	300	350	0.94	5	50.3	52.2	56	142	153
p	300	433	1.07	4	45.1	46.4	48	126	131
p	300	600	1.3	5	39	41.4	44	108	115
p	300	700	1.43	5	36.8	39.4	40	102	108
p	300	850	1.62	5	34.6	37.3	38	95	102
p	300	1195	2.04	4	31.7	33.5	37	87	97.2
e	300	0.98	2.73	4	29.5	31.5	32.5	81.4	87
p	300	114 000	123	4	29.6	31.5	30	85.1	85.5
π	300	29 900	215	4	29.8	31.6	29.6	85.6	85.6
π	300	44 900	322	4	29.8	31.7	29.6	85.7	88.8
				3		30.9		84.9	
		average differences				$\langle r_w \rangle = -1 \pm 6$			$\langle r_p \rangle = -5 \pm 4$
Esbensen *et al.* (1978)									$1.5 \pm 5\%$
p	900	1 280	2.13	4	85.0	85.7		277	279
p	900	5 135	6.4	4.3	73.9	74.9		254	252
p	900	14 100	16	4.3	75.0	75.9		268	259
K	900	5 530	12.1	4	73.5	74.4		260	254
K	900	14 500	30.4	4	74.1	74.9		267	264
π	900	1 865	14.3	4	73.6	74.4		261	262
π	900	5 860	43	4	74.4	75.2	76.4	269	264
π	900	14 900	107	4	75.0	75.8		272	264
		average differences				$\langle r_w \rangle = 1.6$			$\langle r_p \rangle = 1.4 \pm 1.5$

TABLE IX. (*Continued.*)

	t	T	$\beta\gamma$	σ_n	w	w_i	w_x	${}_i\Delta_p$	${}_x\Delta_p$
Nagata *et al.* (1975)							±2.5		≈±1
e	1 565	50	99	10	123.0	126.2	126	484	485
e	1 565	80	158	10	123.3	126.5	129	485	497
e	1 565	100	197	10	123.4	126.5	132	486	487
e	1 565	220	435	10	123.7	126.9	141	487	492
e	1 565	300	590	10	123.7	126.9	129	488	494
e	1 565	390	760	10	123.7	126.9	127	488	492
e	1 565	500	980	10	123.7	126.9	137	488	490
e	1 565	700	1370	10	123.7	126.9	129	488	492
e	1 565	1000	1960	10	123.7	126.9	129	488	489
		average differences				$\langle r_w \rangle = 3 \pm 3.4$		$\langle r_p \rangle = -0.3 \pm 2$	
Nagata *et al.* (1975)							±1%		≈±2%
e	2 905	200	395	20	220.5	227.6	247	935	938
e	2 905	300	590	20	220.6	227.7	255	935	938
e	2 905	500	980	20	220.7	227.8	265	936	928
e	2 905	700	1370	20	220.7	227.8	250	936	943
e	2 905	1000	1960	20	220.7	227.8	245	936	943
e	2 905	1000	1960	45	220.7	254.0	245	936	943
		average differences				$\langle r_w \rangle = 10 \pm 3$		$\langle r_p \rangle = -0.3 \pm 0.7$	
Møller *et al.* (1982)									
e	148	0.976	2.7	3.8	16.25	18.17	18.6	38.4	40.3
e	148	199	391	2.8	17.2	18.43	18.73	40.4	41.4
e^+	148	9 999	19 600	3.4	17.25	19.45	19.31	40.6	39.6
e	148	9 999	19 600	3.4	17.25	19.45	19.42	40.6	39.5
e	148	50 000	98 000	3.3	17.19	19.27	19.86	40.6	39.7
e	290	199	391	2.5	29.08	29.85	29.9	82.2	80.9
e	1 007	199	391	3.4	82.9	83.5	84.9	306	323
		average differences				$\langle r_w \rangle = 1 \pm 1.4$		$\langle r_p \rangle = -0.5 \pm 3.6$	
Ogle *et al.* (1978)									±2.5%
e	100.7	8 200	16 000	2.34	12.9	14.26		26.8	26.4
e	100.7	15 300	30 000	2.34	12.9	14.26		26.8	24.9
e	100.7	24 500	48 000	2.34	12.9	14.26		26.8	25.1
e	100.7	51 100	100 000	2.34	12.9	14.26		26.8	25.1
		average differences						$\langle r_p \rangle = -6 \pm 3$	

the authors' Table II, $\sigma_n = 4 \pm 0.4$ keV (5 ± 0.4 keV), and the Landau variable λ is calculated with

$$\lambda = (\Delta - \Delta_{mp} + 0.225\xi)/\xi \,, \tag{10.3}$$

where Δ is the energy loss and Δ_{mp} and ξ are free parameters given in the authors' Table II (or Table I). Then I determined w_x for these functions. The uncertainty of w_x (±8%) given in Table IX was calculated by repeating the calculation of w_x with the values of δ_2 and ξ both increased by the errors given in the authors' Table II, and with $\sigma_n = 4.4$ keV. The error of Δ_{mp} did not influence w perceptibly. It must be noted that the increase in w by convoluting the noise function with the energy-loss function (seen in columns 5–7 of Table IX) is over 6% for this experiment, and an exact knowledge of σ_n would be desirable in order to achieve a correct theoretical value w_i. Furthermore, I cannot understand the fluctuations in the difference $E_{mp} - \Delta_{mp}$ appearing in the authors' Table II (the differences for the pion data are 1.6, 2.8, and 2.3 keV—my calculations, using the authors' procedure, gave differences of 2.7, 2.4, and 2.7 keV). The separation into pion and proton data shown in the authors' Figs. 3 and 4 is simply an artifact of the choice of the abscissa—it would not appear if the functions were plotted against $\beta\gamma$. The calculation of straggling functions with the free parameters used by the authors (i.e., ξ, Δ_{mp}, and δ_2) must be considered a parameter fit to experimental data without any significance for the understanding of the theory.

Esbensen *et al.* (1978) in their Table IV gave values of Δ_p (with errors) for several particles randomly incident on a silicon detector of thickness 900 μm. As predicted by the present theory, there is no significant difference in the values for particles of opposite charge. The experi-

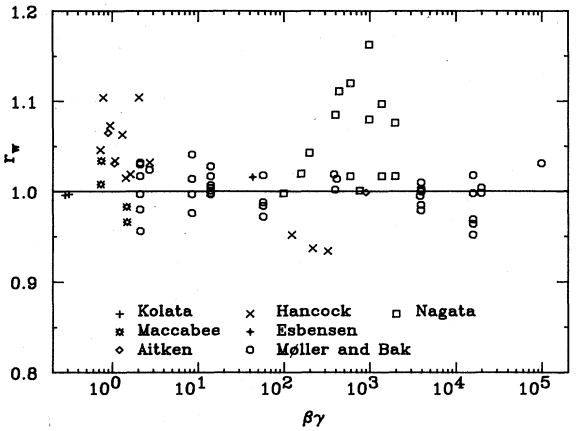

FIG. 16. Comparison of experimental and theoretical values from Tables VIII and IX, of the full width at half maximum w. The abscissa is $\beta\gamma = p/Mc$, where p is the momentum of the incident charged particle, M its rest mass, and c the speed of light. The ratio $r_w = w_x/w_i$ is shown as the ordinate, where w_x is the width of a measured straggling function, and w_i that of the calculated function. The data are for electrons ($Mc^2 = 0.511\,004$ MeV), pions (139.578 MeV), kaons (494 MeV), protons (938.256 MeV), and α particles (3727.328 MeV) passing through silicon detectors of thicknesses between 150 and 3000 μm. Errors are given in the tables.

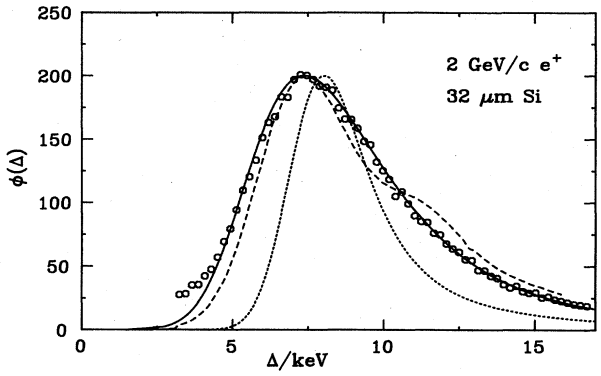

FIG. 18. Ionization functions $\phi(\Delta)$ for 2-GeV/c positrons traversing a silicon detector of thickness 32 μm (Bak *et al.*, 1987). The ionization is represented by the equivalent energy loss Δ, which is the product of W, the average energy needed to produce an electron-hole pair and the number of pairs measured in the experiment. The value of W is implicit in the energy calibration provided by the authors (see Sec. X.C). It is assumed that the energy-deposition curve differs very little from the energy-loss curve. The solid line represents the function $\phi(\Delta)$ calculated with the present theory with a value $\sigma_n = 0.784$ keV, measured in the experiment. For Figs. 18–21, the theoretical functions were normalized to the maximum value of the experimental ones. The circles represent the experimental data; stochastic errors are less than the size of the symbols. The energy scale provided from the experiment has been shifted by 0.22 keV (3%) so as to have the experimental value ${}_x\Delta_p$ and the theoretical value ${}_i\Delta_p$ of the most probable ionization coincide. The calculated value of ${}_i\Delta_p$ is 7.36 keV; the width is $w_i = 5.6$ keV (see Table VIII). The electronic stopping power calculated with Eq. (4.1) is $dT/dt = 4997$ keV/cm; thus the mean energy loss in the detector, $\langle \Delta \rangle = 16$ keV, lies in the tail of the ionization losses shown in the figure. The Vavilov function ($\xi = 0.57$ keV, $\kappa = 5.7 \times 10^{-7}$) convoluted with the noise contribution is shown as the dotted line, with a value of the most probable energy loss of 8 keV (see Appendix E) and with $w = 3.2$ keV. The dashed line is the theoretical function given by Bak *et al.* The difference between theory and experiment for $\Delta < 4$ keV is probably due to a loss of detector sensitivity near the edges. In Table VIII this experiment shows some of the largest differences between theory and experiment.

mental data given in Table IX are therefore a weighted average for the particles of opposite charge. The authors provided me with a plot of the data for 6-GeV/c pions, on which I measured the value of w given in Table IX. It should be noted that there is no relation of the "average energy loss $\langle \Delta E \rangle$" given in the authors' table to the stopping power, Eq. (4.2). $\langle \Delta E \rangle$ appears to be the average value of energy loss calculated from the restricted spectra shown and does not include larger energy losses included in the calculation of stopping power dT/dt. If the upper limit used in the calculation were known, $\langle \Delta E \rangle$ would be a useful datum for the comparison with theory.

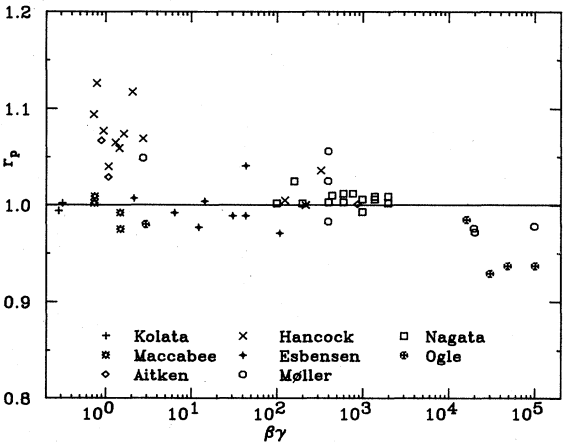

FIG. 17. Comparison of theoretical and experimental values (from Table IX) of the most probable energy loss Δ_p. The abscissa is $\beta\gamma$. The ratio $r_p = {}_x\Delta_p/{}_i\Delta_p$ is shown as the ordinate, where ${}_x\Delta_p$ is the most probable energy loss of a measured straggling function, and ${}_i\Delta_p$ that of the calculated function. The data are for electrons, pions, kaons, protons, and α particles passing through silicon detectors of thicknesses between 150 and 3000 μm. Errors are given in Table IX.

Nagata *et al.* (1975) gave values of the errors of all their experimental data. I suspect, though, that they only included the stochastic uncertainties from counting statistics, but did not consider other sources of random or systematic errors (e.g., electronic noise contributions from the operation of the accelerator or the presence of external radiations, e.g., bremsstrahlung from defining slits). For their thick detector (2.905 mm), the spread in the values of w_x shown in their Table II (reproduced in Table IX) is over 20 keV or 8%, while the error given by

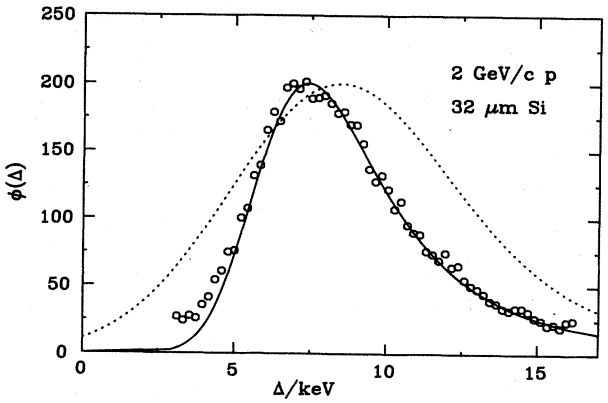

FIG. 19. Ionization functions $\phi(\Delta)$ (see Fig. 18) for 2-GeV/c protons traversing a silicon detector of thickness 32 μm (Bak *et al.*, 1987). The solid line represents the calculation with the present theory with a value $\sigma_n = 0.784$ keV, measured in the experiment. The circles represent the experimental data. Stochastic errors are twice the size of the symbol at $\Delta = 7$ keV. The energy scale provided from the experiment has been shifted by 0.27 keV (3.6%), so that the experimental value ${}_x\Delta_p$ and the theoretical value ${}_t\Delta_p$ of the most probable energy loss coincide. The calculated value of Δ_p is 7.4 keV; the width is $w = 5.2$ keV (see Table VIII). Experiment and theory agree quite well. The stopping power calculated with the theory is $dT/dt = 4011$ keV/cm; thus the mean energy loss in the detector, $\langle\Delta\rangle = 12.8$ keV, lies in the tail of the energy range shown in the figure. The Shulek function, calculated with $\delta_2 = 3044$ keV^2/cm and including the noise contribution, is shown as the dotted line, with a value of the most probable energy loss of 8.46 keV and with $w = 8.88$ keV.

the authors is only $\pm 1\%$; for the thin detector, the spread in w_x is 11% (126–141 keV), and the quoted error is only $\pm 2.4\%$.

On the other hand, the spread in ${}_x\Delta_p$ is comparable to the stated error. Since external noise sources would tend to increase w_x, but would not influence ${}_x\Delta_p$ much, I suspect that such sources were present and their influence was not considered. In particular, the authors did not indicate what the electronic noise contribution was during the measurements with the electrons from the accelerator.

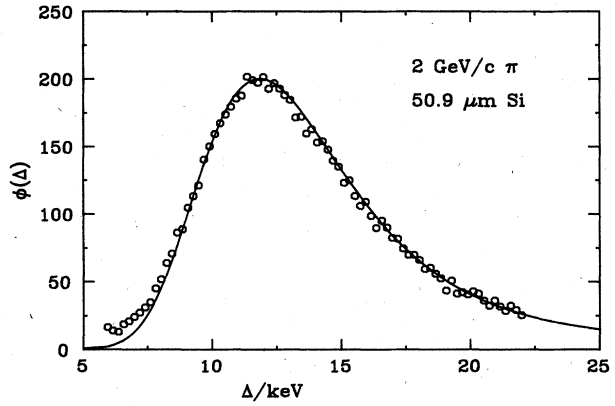

FIG. 20. Ionization function $\phi(\Delta)$ for 2-GeV/c pions traversing a silicon detector of thickness 50.9 μm (Bak *et al.*, 1987). The solid line represents the calculation with the present theory with a value $\sigma_n = 0.73$ keV. The experimental ionization scale was shifted by 0.16 keV. The circles represent the experimental data. The experimental function is slightly narrower than the theoretical one.

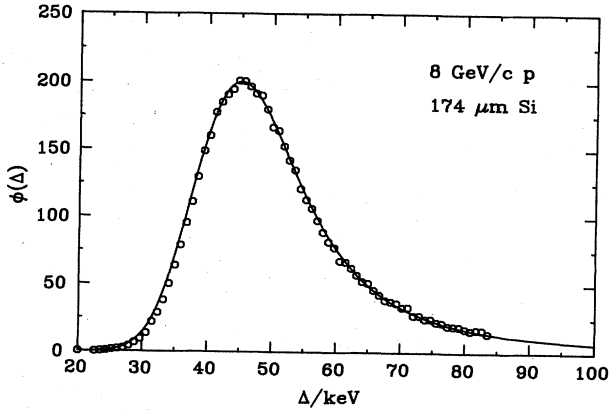

FIG. 21. Ionization function $\phi(\Delta)$ for 8-GeV/c protons traversing a silicon detector of thickness 174 μm (Møller, 1986). The solid line represents the calculation with the present theory with a value $\sigma_n = 3.51$ keV. The ionization scales were not shifted. The circles represent the experimental data. The experimental function is slightly narrower than the theoretical one.

Møller *et al.* (1982): These unpublished data were given to me in the form of plots of the experimental data. Experimental values of w_x and ${}_x\Delta_p$ had been determined by Møller.

Ogle *et al.* (1978): The authors used a value of W of 3.80 eV for their energy calibration. I have multiplied all their values of the most probable energy loss (ε_p in their Table I) by 3.80/3.68, where 3.68 eV was derived in Sec. X.C. The authors did provide an estimated error of 2.5% for their ε_p, but did not give values of w or show any ionization spectra.

The values of r_w for all data points in Table IX are shown in Fig. 16. Except for some of the data of Nagata *et al.* (1975) and the Hancock *et al.* (1983, 1984), no significant difference between theory and experiment is apparent (Appendix I).

The ratios r_p are given in Fig. 17. Except for some measurements by Hancock *et al.* (1983, 1984), and three by Ogle *et al.* (1978), no significant difference between theory and experiment is apparent. The values by Hancock *et al.* also differ substantially from other data at the same range of $\beta\gamma$. The measurements by Ogle *et al.* disagree with the measurement by Møller *et al.* (1982).

Besides the spectra shown in Figs. 18–21, I have compared about 30 complete experimental spectra with theoretical ones. There was a substantial and unexplained difference only for the spectrum of Hancock *et al.* (1983) for 0.736-GeV/c protons [$T = 254$ MeV, their Fig. 2(a)] and for the spectrum for 315-MeV protons given by Aitken *et al.* (1969, see Table IX). Very good agreement was achieved if the noise contribution

σ_n was assumed to be, within reason, an adjustable parameter. For example, the energy-loss spectrum shown by Aitken *et al.* for 458-MeV electrons in a silicon detector 2160 μm thick (their Fig. 5) agrees very closely with the calculated spectrum if $\sigma_n = 20$ keV is assumed (i.e., a Gaussian noise spectrum with $w_n = 50$ keV; see Table IX). With $\sigma_n = 10$ keV, the difference between w_x and w_i is 4%. The authors did not give σ_n. Most of the broadening of the spectrum thus is due to the binding (resonance) effects and the noise. A contribution from internal bremsstrahlung, as postulated by the authors, should occur (Appendix I), but could only be determined from experiment if σ_n were well known. In none of the 30 comparisons were the delta-ray escape or any of the effects (b)–(j) of Sec. IX obviously apparent.

It may be mentioned that in one of the experiments of Møller *et al.* (1982) (not shown in Table IX) a fair amount of radiation from upstream hit the detector, causing a considerable change in the ionization spectrum especially for $\Delta > \Delta_p$. Bak *et al.* (1987) were able to eliminate this problem.

The experimental function given by Baily *et al.* (1983) for 5-GeV/c pions in a silicon detector about 20 μm thick was reviewed earlier by Bichsel (1985a). It is not repeated here because the large uncertainty of the detector thickness does not permit a conclusion about the validity of the theory.

The data given by Julliot and Cantin (1978) are in general agreement with the present theory. Insufficient detail was given in the reference to contribute to a confirmation of the theory.

XI. CONCLUSIONS

It is seen that the present theory of energy loss agrees well with experimental data over a very large range of particle energies ($0.3 \leq \beta\gamma \leq 10^5$), detector thicknesses ($32 \leq t \leq 3000$ μm), and for a variety of particles (electrons, pions, kaons, protons, and α particles). It is the most accurate confirmation of our understanding of the interaction of relativistic charged particles with electronic excitations in matter.

The approximations made in the theory should cause no restrictions in an application for very thin solid absorbers [to the order of 1 μm; for absorbers of thickness of the order of 10 nm, surface plasmons and other effects will appear (Raether, 1980)]. I am not aware of any restriction as far as the energy of the incident particles is concerned.

A variety of effects described in Sec. IX must be considered in the application of the theory of energy losses to experimental measurements of energy deposition and ionization spectra. These effects will be the same for all the energy-loss theories. Many of them are quite unimportant for the experiments reviewed in Sec. X, but they would gain in importance for particles with lower energies and for detectors thinner or thicker than discussed here. The delta-ray escape, for example, will become important for very thin detectors (less than about 5 μm).

For electrons with $T \gg 1$ MeV, internal bremsstrahlung will be of increasing importance with increasing detector thickness above about 1 mm (Appendix I). A detailed treatment of this subject is beyond the scope of this study.

It is evident from Tables V–VII and Figs. 11–13, and 15 that the quality of the results of a straggling theory depends primarily on the quality of the approximation made for the single collision spectrum. Even with the fairly sophisticated approximation used by Allison and Cobb (1980; see Table VII) and by Bak *et al.* (1987), the results are not very good (Fig. 18). Some improvements are desirable for the collision spectrum: better data are needed for the photoabsorption coefficients for $E > 6$ eV, also an improved theory for GOS, especially for M-shell electrons.

It is worth repeating that, while it is possible to obtain a Shulek function with the correct width for thin absorbers (by choosing a suitable value of δ_2, Appendix G), this function will not have the correct shape and the correct value of the most probable energy loss Δ_p. In principle, it may be possible to calculate Shulek functions agreeing exactly with convolution functions, if ξ, Δ_p, and δ_2 are used as adjustable parameters, as suggested by Hancock *et al.* (1983). I have not tried this.

There is still some uncertainty about W. From the discussion in Sec. X.C, it can be concluded that W is constant within about $\pm 2\%$ for the particles and energies represented there. On the other hand, it is known that for low-energy particles (electrons; protons and α particles with energies below 10 MeV) W does depend on particle type and speed (ICRU, 1979; Lennard *et al.*, 1986). Because of these problems caution is necessary with the energy calibration of silicon detectors. In particular, a calibration with natural α particles will not be correct for relativistic particles.

The average standard deviations of w and Δ_p of the experimental data in Table VIII are $\pm 2\%$. The average difference of all experimental values of w and Δ_p from the theoretical ones is less than $\pm 0.2\%$. Thus it will be necessary to perform experiments with much smaller uncertainties (i.e., of the order of 0.2%) if errors of the present theory are to be demonstrated experimentally.

With the present computer program, the calculations of energy-loss functions need slightly more time than calculations with the Shulek function (Appendix D). This is a small disadvantage of the convolution method.

Clearly, the differences between the different theories noted in Figs. 11–15 must be expected for other materials also. These differences were demonstrated theoretically for aluminum by Bichsel and Saxon (1975) and have been observed qualitatively for Al (Perez *et al.*, 1977), Ge (e.g., Esbensen *et al.*, 1978), NaI (Bellamy *et al.*, 1967), xenon (Bichsel, 1974), and other gas detectors (Bichsel, 1985b). A quantitative description for these detectors would require the calculation of the collision spectrum as shown in Sec. III. For argon, the PAI approximation for

$\sigma(E)$ has been given by Allison and Cobb (1980; see Table VII).

I suggest that theoretical values of the most probable energy loss Δ_p and the full width at half maximum w, calculated with the present theory and modified by the considerations of Sec. IX, be used for the calibration of silicon detectors henceforth. Since w and Δ_p depend on t nonlinearly and with different functional behavior (see the values of Δ_p/w in Table VI), it is possible to determine the detector thickness from these two quantities.

ACKNOWLEDGMENTS

I am grateful to Professor Albrecht Kellerer, for explaining the convolution method; Professor Ugo Fano, for helping me understand the Landau theory during our sabbaticals in Berkeley in 1967; Professor Steve Manson, for supplying me (in 1969) with his computer program for the calculation of GOS and for his advice; Dr. Mitio Inokuti, for help and advice; and John Hubbell, for providing me with extensive data tables of x-ray absorption coefficients. I wish to thank the people at the Nuclear Physics Laboratory at the University of Washington for making available the use of the VAX 11-780 for calculations and word processing. The earlier version of the program (based on the PAI approach) was developed at the Physics Department of the University of Aarhus during the winter of 1982, and I am grateful for their hospitality and support.

APPENDIX A: THE KRAMERS-KRONIG RELATION

If, for a given value of momentum transfer K, $\varepsilon_2(E,K)$ is known for all E, the Kramers-Kronig relation permits the calculation of $\varepsilon_1(E,K)$ (Shiles *et al.*, 1980):

$$\varepsilon_1(E,K)=1+\frac{2}{\pi}\int_0^\infty d\omega\frac{\omega\varepsilon_2(\omega,K)}{\omega^2-E^2}\ , \tag{A1}$$

where the principal value of the integral is to be used.

A variety of problems were encountered in the numerical evaluation of this integral, and I made a number of mistakes in early calculations. In particular, for $K=0$, seeing that ε_2 was very small for $E<1.5$ eV, I neglected the contribution from 0 to 1.5 eV. This caused large errors for ε_1 for $E<6$ eV. The following approach gave satisfactory results: for $E<1.5$ eV, ε_2 was approximated by a linear function. The integral from 0 to 1.5 eV then was calculated analytically [Eq. (A2)] and evaluated for each value of E. For large values of E, single-precision calculation (i.e., with 32-bit numbers) gave errors in ε_1 because the difference ω^2-E^2 was very small for $\omega\simeq E$. The integrals therefore were evaluated with double-precision arithmetic.

In order to reduce inaccuracies in the numerical evaluation of the integral in Eq. (A1) for $\omega\simeq E$, the following modification was used:

$$\begin{aligned}\varepsilon_1(E,K)=1&+\frac{2}{\pi}\int_0^{\omega_1}d\omega\frac{\omega\varepsilon_2(\omega,K)}{\omega^2-E^2}\\&+\frac{2}{\pi}\int_{\omega_1}^{\omega_2}d\omega\frac{\omega\varepsilon_2(\omega,K)-E\varepsilon_2(E,K)}{\omega^2-E^2}\\&+\frac{\varepsilon_2(E,K)}{\pi}\left[\ln\left|\frac{\omega_2-E}{\omega_2+E}\right|-\ln\left|\frac{\omega_1-E}{\omega_1+E}\right|\right]\\&+\frac{2}{\pi}\int_{\omega_2}^{\infty}d\omega\frac{\omega\varepsilon_2(\omega,K)}{\omega^2-E^2}\ .\end{aligned} \tag{A2}$$

With this equation, ε_1 was calculated with $\omega_1=1.5$ eV, $\omega_2=20.7$ keV, using 900 steps in between, and analytic solutions for the first and last integral in Eq. (A2). An estimate of the accuracy of the calculation can be obtained from a comparison with the values given by Aspnes and Studna (1983). The final results for $\varepsilon_1(E,0)$ for $1.5\le E/\text{ev}\le 6$ differed by less than 1% from theirs. In the further use of the data, for $E>2300$ eV (where $\varepsilon_1=0.999\,816$) the free-electron approximation of Eq. (2.18) for ε_1 was used, with E_r replaced by $E_a=31.048$ eV.

APPENDIX B: SUM RULES

The following sum rules were used in the final determination of the dielectric functions (Shiles *et al.*, 1980):

$$\frac{2}{\pi E_a^2}\int E\varepsilon_2(E,K)dE=1\ , \tag{B1}$$

$$\frac{2}{\pi E_a^2}\int E\ \mathrm{Im}[-1/\varepsilon(E,K)]dE=1\ , \tag{B2}$$

where $E_a^2=4\pi ne^2/m$, and n is the density of all the electrons in the solid. With a mass density of 2.3290 g/cm^3 for silicon (Henins and Bearden, 1964), the value $E_a=31.048$ eV was obtained. For the dipole oscillator strength, the sum rule

$$\int f(E,0)dE=1 \tag{B3}$$

was used. A further important quantity is the logarithmic mean excitation energy I defined by

$$\ln I=\frac{2}{\pi E_a^2}\int E\ \mathrm{Im}[-1/\varepsilon(E,0)]\ln E\,dE\ . \tag{B4}$$

The parameters used in correcting the theoretical DOS (Sec. II.E.3) were adjusted until the sum rules were fulfilled and $I=174$ eV (Tschalär and Bichsel, 1968) was achieved.

APPENDIX C: COLLISION CROSS SECTION FOR VERY LARGE ENERGIES OF THE INCIDENT PARTICLES

It is interesting to determine the range of energy losses for which the differential collision cross section is practically independent of the energy of the incident particle if

its speed v is almost equal to the speed c of light. This will explain the independence of the most probable energy loss in multiple collisions seen in Fig. 14. Let us consider $\beta^2=1-\delta$, where $\delta=1/\gamma^2$ is a small number (for 200-MeV electrons, $\delta=6\times10^{-6}$; for 5-GeV/c pions, $\delta=8\times10^{-4}$). The total differential collision cross section, Eq. (3.8), consists of three parts: $\sigma(E)=\sigma_l(E)+\sigma_t(E)+\sigma_u(E)$. It is readily seen that $\sigma_l(E)$, Eq. (3.1), as well as $\sigma_u(E)$ for small and intermediate energy losses, Eq. (3.3), will be constant for values of δ sufficiently small. For large energy losses, Eq. (3.7), $\sigma_u(E)$ will depend on $E_M\approx2mc^2\beta^2\gamma^2=2mc^2\beta^2/\delta$ both because of the relativistic correction term, β^2E/E_M, and because of the termination of $\sigma(E)$ at E_M.

For $\sigma_t(E)$, Eq. (3.2), because of the term $(1-\beta^2\varepsilon_1)$ in the logarithm, there will always be a range of energy losses for which $\sigma_t(E)$ will depend on δ. This will be the case whenever δ is greater than $1-\varepsilon_1(E)$. For $E>500$ eV, the terms inside the large square brackets of Eq. (3.2) can be rewritten as follows, using Eq. (2.18) with $E_r=E_a=31.048$ eV:

$$\varepsilon_2\left\{\ln\left[\left[\frac{E_a^2}{E^2}+\delta\right]^2+\varepsilon_2^2\right]^{-1/2}-1\right\}, \tag{C1}$$

where $\varepsilon^2=1$, $\arctan\varphi\approx\varphi$, and $\beta^2=1$ (except in the logarithmic term) have been used. Clearly, for $\delta\ll(E_a/E)^2$, Eq. (C1) does not depend on δ, while it does for $\delta\gg(E_a/E)^2$. A critical energy loss at which $(E_a/E)^2$ is equal to δ can be defined, $E_\delta=E_a/\sqrt{\delta}=\gamma E_a$. For $E>E_\delta$, δ will determine σ_t, which therefore will still depend on speed.

Due to the leading factor ε_2, the contribution of σ_t to σ will decrease rapidly for $E\gg\Theta_K=1.8$ keV, the binding energy of the K shell. Thus, at $E=10$ keV, σ_t is about one-tenth of σ. If we choose $E_\delta=10$ keV (giving $\delta\approx10^{-5}$ or $\gamma=300$) and calculate the values of the term in curly brackets for $\delta=0$ and 10^{-5} (with $\varepsilon_2=1.4\times10^{-5}$), we get the two values 11.98 and 11.63, with a difference of 3%. The total differential cross section, $\sigma(10\text{ keV})$, will thus increase by only 0.3% as γ increases from 300 to ∞. For $\gamma=100$, σ_t is 18% less than for ∞. In the numerical calculations, it was indeed found that the largest change in $\sigma(E)$ with δ occurred near E_δ, and that it was close to the value derived above. At other energy losses, the influence of small δ will be even smaller.

Finally, for $\sigma_u(E)$, Eq. (3.6), even for $\delta<10^{-3}$, the correction term $\beta^2E/E_M\approx\beta^2E/(2mc^2\beta^2\gamma^2)=\delta(E/2mc^2)$ clearly is small for $E<2mc^2=1$ MeV.

Thus, for the absorber thicknesses considered here, the straggling functions are constant to within 1% for $\gamma>300$, the major change being caused by σ_t at energy losses $E\approx\gamma E_a$. This is also true for the total collision cross section M_0, but not for the stopping power M_1: since E_M and thus $\sigma_u(E)$ increases with γ, M_1 will increase [see Eq. (4.4)].

APPENDIX D: CALCULATION OF STRAGGLING FUNCTIONS, "SHULEK FUNCTION"

The straggling functions given by Landau (1944), Blunck and Leisegang (1950), Vavilov (1957), and Shulek *et al.* (1966) can all be calculated with the same equation. This function is given the generic name "Shulek function." For a particle of speed $v=\beta c$ and charge ze traversing an absorber of thickness t, and for a total energy loss Δ, it is given by

$$f(t,\Delta,\delta_2)=\frac{1}{\pi E_M}e^{\kappa(1+\beta^2\Gamma)}\times\int_0^\infty\exp\left[\kappa f_1(y)-\frac{\kappa\delta_2}{kE_M}\frac{y^2}{2}\right]\times\cos[\lambda_1 y+\kappa f_2(y)]dy\ , \tag{D1}$$

with

$$f_1(y)=\beta^2[\ln y-\mathrm{Ci}(y)]-\cos(y)-y\,\mathrm{Si}(y)\ , \tag{D2}$$

$$f_2(y)=y[\ln y-\mathrm{Ci}(y)]+\sin(y)+\beta^2\mathrm{Si}(y)\ , \tag{D3}$$

$$\lambda_1=\kappa\lambda+\kappa\ln\kappa\ .$$

$\mathrm{Si}(y)$ and $\mathrm{Ci}(y)$ are the sine and cosine integral functions (Abramowitz and Stegun, 1964), and

$$\lambda=\langle\lambda\rangle+\frac{\Delta-\langle\Delta\rangle}{\xi}\ , \tag{D4}$$

$$\xi=ZN_a\frac{k}{\beta^2}t=0.017\,825z^2t/\beta^2\text{ keV},\quad t\text{ in }\mu\text{m}\ , \tag{D5}$$

$$\langle\lambda\rangle=-(1-\Gamma)-\beta^2-\ln\kappa\ , \tag{D6}$$

$$\kappa=\xi/E_M\ , \tag{D7}$$

$$E_M=Mc^2\beta^2\gamma^2/[(M/2m)+(2m/M)+\gamma]\ ; \tag{3.6}$$

E_M is the maximum possible energy loss with $\gamma^2=1/(1-\beta^2)$, M and m the rest masses of the heavy particle and the electron, respectively; $\Gamma=0.577\,215$,

$$\langle\Delta\rangle=t\,dT/dt=\xi 2B \tag{D8}$$

is the mean energy loss, dT/dt the stopping power (Sec. IV.B), B the stopping number, Eqs. (4.3) or (4.4), and δ_2 is given by Eq. (4.5) (δ_2 is further discussed in Appendixes G and H).

It is in the general spirit of the approaches of Vavilov and Shulek *et al.* that the moments of the collision spectrum be extracted from the Laplace-transform integral. Thus $\langle\Delta\rangle$ in Eq. (D4) should be defined by Eq. (D8). For heavy ions, B of Eq. (4.3) can properly be used; however, for electrons, it is open to argument what should be used for B (Appendix E).

For the numerical calculations in the present study, 3000 values of the integrand of Eq. (D1) were calculated, linearly spaced in y; the maximum value y_M of the variable y was chosen such as to make the argument of the

exponential function less than -35.

In principle, a different equation, given, for example, by Börsch-Supan (1961), should be used for the Landau function (for which $\delta_2=\kappa=0$). In practice, values calculated with Eq. (D1) with $\delta_2=0$ and $\kappa=10^{-5}$ differ by less than 10^{-4} from the values given by Börsch-Supan for $-2.5\leq\lambda\leq 3.4$. The Blunck-Leisegang function is obtained with $\kappa=0$, $\delta_2\neq 0$. The Vavilov function is obtained for $\delta_2=0$ and arbitrary values of κ (but with the restriction that the absorber thickness must be much less than the range of the particles). For the Shulek *et al.* (1966) function, both δ_2 and κ are greater than zero.

On an elderly IBM-AT computer with floating point accelerator, programmed in FORTRAN, the calculation of 200 values of $f(t,\Delta,\delta_2)$ takes 12 min. The functions $f_1(y)$ and $f_2(y)$ are calculated only once. Thus there seems to be no need for the approximation of the Landau function by a sum of Gaussians or by polynomials used in some publications. This was a reasonable approach in 1950 (Blunck and Leisegang used four Gaussians and had fairly large errors in the tails). Findlay and DuSautoy (1980) used a sum of nine Gaussians, aiming to improve the Blunck and Leisegang approximation. An approximation with polynomials was given by Tabata and Ito (1979). Since the Landau and the Vavilov functions should only be used for thick absorbers, this discussion is somewhat academic.

It is not very difficult to obtain the equivalent of Eq. (D1) for the spectrum of Eq. (3.7), i.e., calculating the straggling function with Laplace transforms for the function $1/E^3$ in addition to that for $1/E^2$. Unsatisfactory results must be expected because the sharp rise of the E^{-3} term with decreasing E (shown by the dashed line in Fig. 8) differs substantially from the realistic spectrum of Fig. 9.

APPENDIX E: MOST PROBABLE ENERGY LOSS Δ_p AND WIDTH w OF THE LANDAU FUNCTION

Landau gave the following equation for the most probable energy loss:

$$
\begin{aligned}
{}_L\Delta_p &= \xi\left[-0.22278+1-\Gamma-\beta^2+\ln\frac{2mc^2\beta^2\gamma^2}{I}\right.\\
&\qquad\left.+\ln\frac{\xi}{I}-\delta\right]\\
&= \xi\left[\ln\frac{2mc^2\beta^2\gamma^2}{I}+\ln\frac{\xi}{I}+0.2000-\beta^2-\delta\right]. \qquad \text{(E1)}
\end{aligned}
$$

Earlier values for the constant 0.2000 were 0.37 (Landau, 1944) and 0.198 [Maccabee and Papworth (1969), quoted by Sternheimer and Peierls (1971);[12] see, also, Ahlen (1980)]. The equation includes the density effect, which had not been used by Landau. It is valid for all particles (Rohrlich and Carlson, 1954), but it does not include any deviations from Eq. (3.5) such as those given in Eq. (3.7) or the Møller terms for electrons and positrons.

For $\gamma\gg 100$, using δ of Eq. (4.9), we get

$$
\begin{aligned}
{}_L\Delta_p &= \xi\left[\ln\frac{2mc^2}{I}+\ln\frac{\xi}{I}-0.8+4.447\right]\\
&= \xi\left[12.325+\ln\frac{\xi}{I}\right]. \qquad \text{(E2)}
\end{aligned}
$$

If we enter the I value and Eq. (D5) for ξ, we obtain

$$
{}_L\Delta_p(\text{keV}) = t(0.1791+0.017\,82\ln t)\,, \qquad \text{(E3)}
$$

with t in μm (compare to Table V). We note that the addition of δ_2 to the Landau function in the mixed methods increases the values of ${}_L\Delta_p$.

Substantially different results (especially for electrons) would be obtained if Eq. (D4), together with the standard stopping-power values (Table V), were to be used.

The small values of r_p for small t in Table V can be understood qualitatively: for very thin absorbers, K-shell electrons do not contribute to the energy loss. Thus, the effective thickness of the absorber can be considered to be $t_e=\frac{12}{14}t$. For $t=10$ μm, $t_e=8.57$ μm, and we calculate ${}_L\Delta_p=1.863$ keV, which is close to the value $\Delta_p=1.857$ keV in Table V.

For the Landau function, the full width at half maximum w depends on the absorber thickness and is independent of particle type and speed. The exact value is $w_L=4.018\xi$. For the Vavilov functions, w_V depends on t and the particle speed, which is usually represented by the parameter κ. For $\kappa<0.1$, w_V is the same as w_L. For increasing values of κ, w_V decreases gradually, reaching a value 2.3ξ at $\kappa=1$. For the sake of simplicity, $w_L=4\xi$ has been used in this paper.

APPENDIX F: THE BLUNCK-LEISEGANG FUNCTION

A calculation of the straggling function with the unbounded Rutherford cross section, $\sigma(E)=k/E^2$, $0\leq E\leq\infty$, would lead to divergent integrals. Both Landau (1944) and Vavilov (1957) circumvented this problem by essentially extracting the first moment M_1 from the first Laplace transform needed in their treatment. In order to achieve a better approximation, Blunck and Leisegang (1950) also extracted the second moment and arrived at the equivalent of Eq. (D1) for $\kappa=0$. In order to avoid the tedious calculations of that equation, they derived the following equation, using the convolution theorem for Fourier integrals:

$$
\begin{aligned}
f(t,\Delta,\delta_2) &= \frac{1}{(2\pi t\delta_2)^{1/2}}\\
&\quad\times\int_{-\infty}^{\infty} f_L(\Delta-y)\exp[-y^2/(2t\delta_2)]dy\,, \qquad \text{(F1)}
\end{aligned}
$$

[12]References to Sternheimer's earlier work will be found in this paper.

where f_L is the Landau function. This equation can thus be considered a "mixed-method" approach. It may be noted that the quantity K_r^2 in the Blunck and Leisegang formulation is equal to δ_2.

Shulek *et al.* (1967) also extracted M_2 and arrived at Eq. (D1). Bichsel (1970a) showed that it is not practical to extend the approach to higher moments, and also showed where and how the approximation of Shulek *et al.* will break down (see Fig. 8 of Bichsel, 1970a).

Straggling functions have been calculated with both Eqs. (D1) and (F1). If, rather than using tabulated values, the Vavilov function is calculated with Eq. (D1) before the convolution of Eq. (F1) is performed, it is more efficient to use Eq. (D1) from the beginning [preferably including the noise contribution in δ_2 (Hancock *et al.*, 1983)].

APPENDIX G: VALUES OF δ_2

Those readers who believe that the Blunck-Leisegang (1950) or Shulek *et al.* (1966) methods provide a viable approach to the calculation of straggling functions (Appendixes D and F) should consider the following thoughts about δ_2. In the calculation of an energy-loss spectrum $f(\Delta)$, any energy losses $E>\Delta$ in the primary collision spectrum cannot contribute to $f(\Delta)$. This can readily be seen in the convolution approach, Eq. (7.1). Any deviation from the Rutherford spectrum for energy losses $E>\Delta$ is irrelevant to the calculation of $f(\Delta)$. The upper limit of the integrals in Eqs. (4.1) and (4.7) used for the calculation of δ_2 therefore should be Δ rather than E_M. While $\delta_2(\Delta)$ can readily be obtained at the same time that $\sigma(E)$ is calculated, it would be rather tedious to introduce these values into the calculation of Eq. (D1), and this is something which I have not done. This approach would break down for absorbers thinner than about 10 μm, where the structure of the single collision spectrum would be important (Bichsel and Saxon, 1975).

An easy approach to get a single order-of-magnitude value of δ_2 would be to calculate δ_2 up to $E_\delta=\Delta_p$, the most probable energy loss. For example, for 45-GeV/c pions passing through a silicon detector 300 μm thick, $\Delta_p\approx 85$ keV. Then δ_2 for $E_\delta=85$ keV is 1930 keV^2/cm. This is not much larger than the value $\delta_2=1794$ keV^2/cm used in Fig. 13 to achieve a function with the same width as the function from the present theory. This approach also works for electrons and positrons, since the terms in E/T seen in Uehling's (1954) Eqs. (9) and (10) ($E/T=Q/E_K$) are small for energy losses small compared to T.

Another example: 1-GeV electron passing through a silicon detector 10 μm thick, $\Delta_p\approx 1.85$ keV. Then δ_2 for $E_\delta=1.85$ keV is 368 keV^2/cm. Again, this is not much larger than the value $\delta_2=359$ keV^2/cm used in Fig. 11 to achieve a function with the same width as the function from the present theory.

Values of δ_2 calculated with this approach may give a function with a width w close to the correct one, but the function $f(\Delta)$ still will rise too slowly below Δ_p and drop too fast above (see Figs. 11–13). The reader, at his own risk, may try this approach.

APPENDIX H: CALCULATION OF δ_2 ACCORDING TO SHULEK AND FANO

In their Eq. (8), Shulek *et al.* (1966) used the following second moment of the straggling function (their notation):

$$\omega=\xi\left[E_M(1-\beta^2/2)(Z_{\rm eff}/Z)+\sum \tfrac{8}{3}I_i f_i \ln\frac{2mc^2\beta^2}{I_i}\right], \tag{H1}$$

where, for present purposes, $Z_{\rm eff}=Z$, I_i is the excitation energy for atomic shell i, and f_i the corresponding oscillator strength. This equation was modified by the authors from Eqs. (787a) and (788) of Livingston and Bethe (1937) to include relativistic effects. ω is equal to tM_2, with M_2 given by Eq. (4.1). The first term in the large parentheses, multiplied by $k_s=N_a k/\beta^2$, is exactly M_2', Eq. (4.6), with $\xi=k_s t$. The second term is δ_2:

$${}_S\delta_2=k_s\sum \tfrac{8}{3}I_i f_i \ln\frac{E_M}{I_i}\ . \tag{H2}$$

It is not obvious whether the value $2mv^2$ in the Livingston-Bethe equations should be replaced by $E_M=2mc^2\beta^2$ or by Eq. (3.6). Furthermore, Eq. (H2) is a rather rough approximation. Fano derived his Eq. (72), expressed here as

$${}_F\delta_2=k_s\tfrac{2}{3}\left\langle\left|\sum_j v_j\right|^2\right\rangle_0 \ln\frac{2mc^2\beta^2}{I_1}\ , \tag{H3}$$

where I_1 is defined by

$$\ln I_1=\int E\ln E\ \mathrm{Im}[-1/\varepsilon(E,0)]dE\Big/\int E\ \mathrm{Im}[-1/\varepsilon(E,0)]dE \tag{H4}$$

rather than the customary I value (174 eV), Eq. (B4). For silicon, $I_1=2480$ eV. I have not been able to evaluate the term

$$\left\langle\left|\sum_j v_j\right|^2\right\rangle_0$$

used in Fano's Eq. (72), and therefore cannot give a value of δ_2 calculated with this equation (see Bichsel, 1974, for an approximation). Values used so far (e.g., Hancock *et al.*, 1983) for Eq. (H2) are given in Table X, together with those needed in Eq. (H3), given by Inokuti *et al.* (1978). The large differences between I_i and I_{1i} indicate that ${}_S\delta_2$ provides only a rough estimate of the value.

Since Livingston-Bethe, Sternheimer, and Fano in

TABLE X. Values of f_i and I_i (eV) for Eq. (H2) from Sternheimer (1966) and of f_I and I_{1i} (eV) for Eq. (H3) from Inokuti *et al.* (1978). Values of ${}_S\delta_2$ (keV^2/cm^2) for 45-GeV/c pions, calculated with $E_M=2mc^2\beta^2$ (column 6) and E_M from Eq. (3.6) (column 7); $k=178.25$ keV/cm.

Shell	f_i	I_i	f_I	I_{1i}	${}_S\delta_2$	
Column 1	2	3	4	5	6	7
K	$\frac{2}{14}$	1841	1.6/14	5780	790	2082
L	$\frac{8}{14}$	112	8.4/14	608	278	593
M_1	$\frac{2}{14}$	41	$\frac{4}{14}$	460	28	57
M_2	$\frac{2}{14}$	12			9	18
total					1105	2750

their studies all used the ratio $M_2/M_2'=1+(\delta_2/M_2')$, they apparently assumed that $D_2=\delta_2/M_2'$ would be so small for relativistic particles that it could be neglected, and that the approximation $E_M=2mv^2$ would be adequate for all purposes. It will be seen in the example below that D_2 indeed is very small, but there will still be a large correction to the Landau function for thin absorbers. Values of δ_2 calculated with $E_M=2mc^2\beta^2$ and with the value of E_M from Eq. (3.6) are given in Table X. As expected, ${}_S\delta_2(2mv^2)$ (column 6) is much less than ${}_S\delta_2(E_M)$ (column 7). The value of δ_2 calculated with Eqs. (3.7) and (4.5) is 3270 keV^2/cm, even larger than the result (footnote 6) of column 7. The remarks about the usefulness of δ_2 made in Appendix G still apply.

It may be noted that the value used by Hancock *et al.* (1983) in their Fig. 4 is the value from the sixth column of the table, $\delta_2=1105$ keV^2/cm (their $\delta_2=33$ keV^2 is this value multiplied by the absorber thickness $t=0.03$ cm; see Fig. 13), thus an incorrect theoretical value gave apparent agreement with experiment. The value of $D_2=\delta_2/M_2'=1.7\times10^{-6}$ for this case is indeed very small (as anticipated above), but since for a 300-μm silicon detector this is larger than $\kappa=1.7\times10^{-7}$, it will considerably broaden the straggling function.

APPENDIX I: INFLUENCE OF INTERNAL BREMSSTRAHLUNG ON IONIZATION FUNCTIONS

For the thin absorbers under consideration in this paper, bremsstrahlung need be considered only for incident electrons and not for the heavier ions. A difference must be expected between the energy-loss spectrum, including the bremsstrahlung loss, and the energy deposition spectrum, because a considerable fraction of the bremsstrahlung photons will escape from the detector. For example, in a 100-μm silicon detector, less than one-half of all bremsstrahlung photons with energy of 10 keV produced in the detector would be absorbed in it; for 20-keV photons, no more than 5% would be absorbed.

For incident electrons with an energy of 1 GeV, the energy loss due to bremsstrahlung is 104 MeV/cm compared to 4.9 MeV/cm for the energy loss due to inelastic collisions (ICRU, 1984). The radiative energy loss to photons with energies less than 100 keV is only 0.011 MeV/cm, though, or 0.2% of the collision loss [this estimate was obtained from Eq. (27) and Fig. 14 in Heitler (1944)]. According to Seltzer and Berger (1985), the value is 0.015 MeV/cm. Thus we can expect that the effect of bremsstrahlung will be quite small for the detectors under consideration.

Quantitative results for the energy loss have been presented by Blunck and Westphal (1951) in their Figs. 2 and 3. The quantity $\alpha=0.001\,40\times(Z^2/A)\rho\times[\frac{4}{3}\ln(183/Z^{-(1/3)})+\frac{1}{9}]$ cm^{-1} is equal to 0.134 cm^{-1} for silicon. For the thicker absorber in Nagata *et al.* (1975), $R=0.29$ cm, αR thus is 0.04, and, from Fig. 3 of Blunck and Westphal, the increase in the full width at half maximum w of the energy-loss function is approximately 6%. Only a fraction of this increase will occur in the ionization spectrum. The effect therefore is of the same order of magnitude as the contributions of resonance and noise (Table IX). The bremsstrahlung contribution seems to be too little to explain the relatively large values of r_w in Fig. 16 for this absorber. Berger *et al.* (1969) have discussed the problem for thicker absorbers.

REFERENCES

Abramowitz, M., and I. A. Stegun, 1964, Eds., *Handbook of Mathematical Functions,* National Bureau of Standards, Applied Mathematical Series No. 55 (U.S. GPO, Washington, D.C.).

Ahlen, S. P., 1980, Rev. Mod. Phys. **52**, 121.

Aitken, D. W., W. L. Lakin, and H. R. Zulliger, 1969, Phys. Rev. **179**, 393.

Allison, W. W. M., and J. H. Cobb, 1980, Annu. Rev. Nucl. Part. Sci. **30**, 253.

Anholt, R., 1979, Phys. Rev. A **19**, 1004.

Antončik, E., G. di Cola, and L. Farese, 1970, Radiat. Eff. **5**, 1.

Ashley, J. C., 1982, J. Electron. Spectrosc. Relat. Phenom. **28**, 177.

Ashley, J. C., R. H. Ritchie, and W. Brandt, 1972, Phys. Rev. A **8**, 2402.

Aspnes, D. E., and A. A. Studna, 1983, Phys. Rev. B **27**, 985.

Baily, R., C. J. S. Damerell, R. L. English, A. R. Gillman, A. L. Lintern, S. J. Watts, and F. J. Wickens, 1983, Nucl. Instrum. Methods **213**, 201.

Bak, J. F., A. Burenkov, J. B. B. Petersen, E. Uggerhøj, S. P. Møller, and P. Siffert, 1987, Nucl. Phys. B **288**, 681.

Bearden, J. A., and A. F. Burr, 1967, Rev. Mod. Phys. **39**, 125.

Bellamy, E. H., R. Hofstadter, W. L. Lakin, J. Cox, M. L. Perl, W. T. Toner, and T. F. Zipf, 1967, Phys. Rev. **164**, 417.

Berger, M. J., S. M. Seltzer, S. E. Chappell, J. C. Humphreys, and J. W. Motz, 1969, Nucl. Instrum. Methods **69**, 181. The differences between measured and calculated spectra are at least partly explained by the ratio $r_p(e)$ of Table V.

Bethe, H., 1930, Ann. Phys. (Leipzig) **5**, 325.

Bethe, H. A., L. M. Brown, and M. C. Walske, 1950, Phys. Rev. **79**, 413.

Bichsel, H., 1968, in *Fundamentals,* Vol. I of *Radiation Dosimetry,* edited by F. H. Attix and W. C. Roesch (Academic,

New York/London), p. 157.
Bichsel, H., 1970a, Phys. Rev. B **1**, 2854.
Bichsel, H., 1970b, Nucl. Instrum. Methods A **78**, 277.
Bichsel, H., 1972, in *American Institute of Physics Handbook,* 3rd ed., edited by D. E. Gray (McGraw-Hill, New York), p. 8-142.
Bichsel, H., 1974, Phys. Rev. A **9**, 571.
Bichsel, H., 1985a, Nucl. Instrum. Methods A **235**, 174.
Bichsel, H., 1985b, Radiat. Protection Dosimetry **13**, 91.
Bichsel, H., 1987, Helv. Phys. Acta **60**, 771.
Bichsel, H., K. M. Hanson, and M. E. Schillaci, 1982, Phys. Med. Biol. **27**, 959.
Bichsel, H., and M. Inokuti, 1976, Radiat. Res. **67**, 613.
Bichsel, H., R. F. Mozley, and W. A. Aron, 1957, Phys. Rev. **105**, 1788.
Bichsel, H., and L. E. Porter, 1982, Phys. Rev. A **25**, 2499.
Bichsel, H., and R. P. Saxon, 1975, Phys. Rev. A **11**, 1286.
Bichsel, H., and S. Yu, 1972, IEEE Trans. Nucl. Sci. **19** (6), 172.
Bloch, F., 1933, Z. Phys. **81**, 363.
Blunck, O., and S. Leisegang, 1950, Z. Phys. **128**, 500.
Blunck, O., and K. Westphal, 1951, Z. Phys. **130**, 641.
Börsch-Supan, W., 1961, J. Res. Nat. Bur. Stand., Sec. B **65**, 245.
Bohr, N., 1948, Dan. Mat. Fys. Medd. **18**, No. 8 (second edition, 1953).
Brenner, D. J., M. Zaider, J. F. Dicello, and H. Bichsel, 1981, in *Proceedings of the 7th Symposium on Microdosimetry,* edited by J. Booz, H. G. Ebert, and H. D. Hartfiel (Harwood, London), p. 677.
Brown, F. C., R. Z. Bachrach, and M. Skibowski, 1977, Phys. Rev. B **15**, 4781.
Chechin, V. A., L. P. Kotenko, G. I. Merson, and V. C. Yermilova, 1972, Nucl. Instrum. Methods **98**, 477.
Chechin, V. A., and V. C. Ermilova, 1976, Nucl. Instrum. Methods **136**, 551.
Chen, C. H., A. E. Meixner, and R. M. Kincaid, 1980, Phys. Rev. Lett. **44**, 951.
Choi, B.-H., E. Merzbacher, and G. S. Khandelwal, 1973, At. Data **5**, 291.
Clementi, E., and D. L. Raimondi, 1963, J. Chem. Phys. **38**, 2686.
Cobb, J. H., W. W. M. Allison, and J. N. Bunch, 1976, Nucl. Instrum. Methods **133**, 315.
Croitoru, N., P. G. Rancoita, and A. Seidman, 1985, Nucl. Instrum. Methods A **234**, 443.
Davidović, D. M., B. L. Moiseiwitsch, and P. H. Norrington, 1978, J. Phys. B **11**, 847.
Dehmer, J. L., M. Inokuti, and R. P. Saxon, 1975, Phys. Rev. A **12**, 102. Dr. Saxon kindly gave me tables of DOS.
Del Grande, N. K., 1986, private communication.
Eisen, F. H., G. J. Clark, J. Bøttiger, and J. M. Poate, 1972, Radiat. Eff. **13**, 93.
Ermilova, V. C., L. P. Kotenko, and G. I. Merzon, 1977, Nucl. Instrum. Methods **145**, 555.
Ershov, O. A., and A. P. Lukirskii, 1966, Fiz. Tverd. Tela Leningrad **8**, 2137 [Sov. Phys. Solid State **8**, 1699 (1967)].
Esbensen, H., O. Fich, J. A. Golovchenko, S. Madsen, H. Nielsen, H. E. Schiøtt, E. Uggerhøj, C. Vraast-Thomsen, G. Charpak, S. Majewski, G. Odyniec, G. Petersen, F. Sauli, J. P. Ponpon, and P. Siffert, 1978, Phys. Rev. B **18**, 1039.
Evans, R. D., 1967, *The Atomic Nucleus,* eleventh printing (McGraw-Hill, New York).
Fano, U., 1963, Annu. Rev. Nucl. Sci. **13**, 1.
Fano, U., and J. W. Cooper, 1968, Rev. Mod. Phys. **40**, 441.
Ferrell, R. A., 1956, Phys. Rev. **101**, 554.
Findlay, D. J. S., and A. R. DuSautoy, 1980, Nucl. Instrum. Methods **174**, 531.
Gähwiller, C., and F. C. Brown, 1970, Phys. Rev. B **2**, 1918.
Geretschläger, M., 1987, Nucl. Instrum. Methods B **28**, 289.
Gerward, L., 1981, J. Phys. B **14**, 3389.
Gerward, L., 1982, *High Precision X-Ray Attenuation Coefficients Measured by an Energy Dispersive Method. Revised Values for Si, Cu and Graphite* (Technical University of Denmark, Lyngby), LTF III Report No. 40.
Hall, G., 1984, Nucl. Instrum. Methods **220**, 356.
Hancock, S., F. James, J. Movchet, P. G. Rancoita, and L. VanRossum, 1983, Phys. Rev. A **28**, 615.
Hancock, S., F. James, J. Movchet, P. G. Rancoita, and L. VanRossum, 1984, Nucl. Instrum. Methods Phys. Res. B **1**, 16.
Hanke, C. C., and H. Bichsel, 1970, K. Dan. Vidensk. Selsk. Mat. Fys. Medd. **38**, No. 3.
Heitler, W., 1944, *The Quantum Theory of Radiation,* 2nd ed. (Oxford University, London).
Henins, I., and J. A. Bearden, 1964, Phys. Rev. A **135**, 890.
Herman, F., and S. Skilman, 1963, *Atomic Structure Calculations* (Prentice-Hall, Englewood Cliffs).
Herring, J. R., and E. Merzbacher, 1957, J. Elisha Mitchell Sci. Soc. **73**, 267.
Hinz, H.-J., 1979, "Elektronenenergieverlustmessungen an Si, Ge und Al. . . .," Dissertation (Universität Hamburg).
Hinz, H.-J., and H. Raether, 1979, Thin Solid Films **58**, 281.
Hunter, W. R., 1966, in *Optical Properties and Electronic Structure of Metals and Alloys,* Proceedings of the International Colloquium on the Optical Properties and Electronic Structure of Metals and Alloys, edited by F. Abelès (North-Holland, Amsterdam), p. 136.
Hunter, W. R., 1985, private communication.
ICRU, 1979, *Average Energy Required to Produce an Ion Pair* (International Commission on Radiation Units and Measurements, Bethesda, MD), Report No. 31. As used in Sec. IX, W is the "differential value w" on p. 1 of the reference.
ICRU, 1984, *Stopping Powers for Electrons and Positrons* (International Commission on Radiation Units and Measurements, Bethesda, MD), Report No. 37.
Inokuti, M., 1971, Rev. Mod. Phys. **43**, 297.
Inokuti, M., Y. Itikawa, and J. E. Turner, 1978, Rev. Mod. Phys. **50**, 23.
Inokuti, M., T. Baer, and J. L. Dehmer, 1978, Phys. Rev. A **17**, 1229.
Inokuti, M., and D. Y. Smith, 1982, Phys. Rev. B **25**, 61.
Ispirian, K. A., A. T. Margarian, and A. M. Zverev, 1974, Nucl. Instrum. Methods **117**, 125.
Jackson, J. D., and R. L. McCarthy, 1972, Phys. Rev. B **6**, 4131.
Jellison, G. E., and F. A. Modine, 1983, Phys. Rev. B **27**, 7466.
Julliot, C., and M. Cantin, 1978, Nucl. Instrum. Methods **157**, 235.
Kellerer, A. M., 1968, *Mikrodosimetrie* (Strahlenbiologisches Institut der Universität München), G. S. F. Bericht B-1.
Knop, G., A. Minten and B. Nellen, 1961, Z. Phys. **165**, 533.
Kohlhaas, E., and F. Scheiding, 1969, in *Proceedings of the 5th International Congress on X-Ray Optics and Microanalysis,* Tübingen, edited by G. Möllenstedt and K. H. Gaukler (Springer, Berlin), p. 193.
Kolata, J. J., T. M. Amos, and Hans Bichsel, 1968, Phys. Rev. **176**, 484.
Lægsgaard, Erik, 1982, private communication.
Landau, L., 1944, J. Phys. (Moscow) **VIII**, 201.
Lapique, F., and F. Piuz, 1980, Nucl. Instrum. Methods **175**,

297.
Laulainen, N., and H. Bichsel, 1972, Nucl. Instrum. Methods **104**, 531.
Lennard, W. N., H. Geissel, K. B. Winterbon, D. Phillips, T. K. Alexander, and J. S. Forster, 1986, Nucl. Instrum. Methods A **248**, 454.
L'Hoir, A., 1984, Nucl. Instrum. Methods **223**, 336.
Lindhard, J., and A. Winther, 1964, K. Dan. Vidensk. Selsk. Mat. Fys. Medd. **34**, No. 4.
Livingston, M. S., and H. A. Bethe, 1937, Rev. Mod. Phys. **9**, 245.
Louie, S. G., J. R. Chelikowski, and M. L. Cohen, 1975, Phys. Rev. Lett. **34**, 155.
Maccabee, H. D., and D. G. Papworth, 1969, Phys. Lett. A **30**, 241.
Maccabee, H. D., M. R. Raju, and C. A. Tobias, 1968, Phys. Rev. **165**, 469.
Manson, S. T., 1972, Phys. Rev. A **6**, 1013.
McGuire, E. J., 1986, Phys. Rev. A **33**, 3572.
McGuire, E. J., J. M. Peek, and L. C. Pitchford, 1982, Phys. Rev. A **26**, 1318.
Miller, J. H., L. H. Toburen, and S. T. Manson, 1983, Phys. Rev. A **27**, 1337.
Møller, S. P., 1986, "Experimental investigations of energy loss and straggling together with inner shell-excitations of relativistic projectiles in solids," Ph.D. thesis (University of Aarhus).
Møller, S. P., *et al.*, 1982, private communication.
Nagata, K., T. Doke, J. Kikuchi, N. Hasebe, and A. Nakamoto, 1975, Jpn. J. Appl. Phys. **14**, 697.
Ogle, W., P. Goldstone, C. Gruhn, and C. Maggiore, 1978, Phys. Rev. Lett. **40**, 1242.
Perez, J. Ph., J. Sevely, and B. Jouffrey, 1977, Phys. Rev. A **16**, 1061.
Philipp, H. R., 1972, J. Appl. Phys. **43**, 2835.
Press, W. H., B. P. Flannery, S. A. Teukolsky, and W. T. Vetterling, 1986, *Numerical Recipes* (Cambridge University, New York), p. 191.
Raether, H., 1980, *Excitation of Plasmons and Interband Transitions by Electrons,* Springer Tracts in Modern Physics, Vol. 88 (Springer, Berlin/Heidelberg/New York).
Ritsko, J. J., S. E. Schnatterly, and P. C. Gibbons, 1974, Phys. Rev. Lett. **32**, 671.
Rohrlich, F., and B. C. Carlson, 1954, Phys. Rev. **93**, 38.
Schimmerling, W., S. Kaplan, T. S. Subramanian, W. J. McDonald, G. Gabor, A. Sadoffi, and E. Alpen, 1983, in *Proceedings of the 8th Symposium on Microdosimetry,* edited by J. Booz and H. G. Ebert (Commission of the European Communities, Luxembourg), p. 311.
Scott, W. T., 1963, Rev. Mod. Phys. **35**, 231.
Seltzer, S. M., and M. J. Berger, 1985, Nucl. Instrum. Methods B **12**, 95.
Shiles, E., T. Sasaki, M. Inokuti, and D. Y. Smith, 1980, Phys. Rev. B **22**, 1612.
Shiles, E., and D. Y. Smith, 1983, private communication.
Shulek, P., B. M. Golovin, L. A. Kulyukina, S. V. Medved', and P. Pavlovich, 1966, Yad. Fiz. **4**, 564 [Sov. J. Nucl. Phys. **4**, 400 (1967)].
Sternheimer, R. M., 1966, Phys. Rev. **145**, 247.
Sternheimer, R. M., and R. F. Peierls, 1971, Phys. Rev. B **3**, 3681. References to Sternheimer's earlier work will be found in this paper.
Sternheimer, R. M., S. M. Seltzer, and M. J. Berger, 1982, Phys. Rev. B **26**, 6067.
Sternheimer, R. M., M. J. Berger, and S. M. Seltzer, 1984, At. Data Nucl. Data Tables **30**, 261.
Stiebling, J., and H. Raether, 1978, Phys. Rev. Lett. **40**, 1293.
Storm, E., and H. I. Israel, 1970, Nucl. Data Tables A **7**, 565.
Sturm, K., and L. E. Oliveira, 1980, Phys. Rev. B **22**, 6268.
Symon, K. R., 1948, "Fluctuations in energy lost by high energy charged particles in passing through matter," Ph. D. thesis (Harvard University).
Tabata, T., and R. Ito, 1979, Nucl. Instrum. Methods **158**, 521.
Talman, R., 1979, Nucl. Instrum. Methods **159**, 189.
Tarrio, C., and S. E. Schnatterly, 1986a, Bull. Am. Phys. Soc., Ser. 2, **31**, 350.
Tarrio, C., and S. E. Schnatterly, 1986b, private communication.
Tomboulian, D. H., and D. E. Bedo, 1956, Phys. Rev. **104**, 590.
Tschalär, C., 1968a, Nucl. Instrum. Methods **61**, 141.
Tschalär, C., 1968b, Nucl. Instrum. Methods **64**, 237.
Tschalär, C., and Hans Bichsel, 1968, Phys. Rev. **175**, 476.
Tung, C. J., R. H. Ritchie, J. C. Ashley, and V. E. Anderson, 1976, *Inelastic Interactions of Swift Electrons in Solids* (Oak Ridge National Laboratory, Oak Ridge), Report No. ORNL-TM-5188.
Uehling, E. A., 1954, Annu. Rev. Nucl. Sci. **4**, 315.
Vavilov, P. V., 1957, Zh. Eksp. Teor. Fiz. **32**, 920 [Sov. Phys.–JETP **5**, 749 (1957)].
Veigele, Wm. J., 1973, At. Data Tables **5**, 51.
Viña, L., and M. Cardona, 1984, Phys. Rev. B **29**, 6739.
Walske, M. C., 1952, Phys. Rev. **88**, 1283.
Williams, E. J., 1929, Proc. R. Soc. London, Ser. A **125**, 420.